ACCSCIENCE PUBLISHING

International Journal of Bioprinting

REVIEW ARTICLE

Microfluidic fiber spinning for 3D bioprinting: Harnessing microchannels to build macrotissues

Federico Serpe[1,2], Carlo Massimo Casciola[2], Giancarlo Ruocco[1], Gianluca Cidonio[1]*, and Chiara Scognamiglio[1]*

[1]Centre for Life Nano- & Neuro-Science (CLN2S), Italian Institute of Technology (IIT), 00161 Rome, Italy

[2]Department of Mechanical and Aerospace Engineering (DIMA), University of Rome "La Sapienza," 00185 Rome, Italy

(This article belongs to the *Special Issue: Advancements in 3D Printing, Microfluidics, and Their Integrated Applications*)

Abstract

Microfluidics is rapidly revolutionizing the scientific panorama, providing unmatched high-throughput platforms that find application in numerous areas of physics, chemistry, biology, and materials science. Recently, microfluidic chips have been proposed, in combination with bioactive materials, as promising tools for spinning cell-laden fibers with on-demand characteristics. However, cells encapsulated in filaments produced via microfluidic spinning technology are confined in a quasi-three-dimensional (3D) environment that fails to replicate the intricate 3D architecture of biological tissues. Thanks to the recent synergistic combination of microfluidic devices with 3D bioprinting technologies that enable the production of sophisticated microfibers serving as the backbone of 3D structures, a new age of tissue engineering is emerging. This review looks at how combining microfluidics with 3D printing is contributing to the biofabrication of relevant human substitutes and implants. This paper also describes the whole manufacturing process from the production of the microfluidic tool to the printing of tissue models, focusing on cutting-edge fabrication technologies and emphasizing the most noticeable achievements for microfluidic spinning technology. A theoretical insight for thixotropic hydrogels is also proposed to predict the fiber size and shear stress developing within microfluidic channels. The potential of using microfluidic chips as bio-printheads for multi-material and multi-cellular bioprinting is discussed, highlighting the challenges that microfluidic bioprinting still faces in advancing the field of biofabrication for tissue engineering and regenerative medicine purposes.

Keywords: Microfluidic; 3D bioprinting; Fiber spinning; Biofabrication

***Corresponding authors:**
Chiara Scognamiglio (chiara.scognamiglio@iit.it)

Gianluca Cidonio (gianluca.cidonio@iit.it)

Citation: Serpe F, Casciola CM, Ruocco G, Cidonio G, Scognamiglio C. Microfluidic fiber spinning for 3D bioprinting: Harnessing microchannels to build macrotissues. *Int J Bioprint*. 2023; 2024;10(1):1404
doi: 10.36922/ijb.1404

Received: July 27, 2023
Accepted: August 25, 2023
Published Online: January 2, 2024

1. Introduction

Microfluidics aims to investigate the physics of static and dynamic fluids at the microscale level. The ability to manipulate small volumes of fluids with high precision provides unparalleled possibilities for the development of novel solutions to interdisciplinary challenges, particularly in the fields of biology, chemistry, physics, and engineering.[1,2]

Microfluidic technologies have encouraged the creation of innovative approaches for fiber spinning. Microfluidic spinning technology (MST) is an advanced method to fabricate microfibers made of biocompatible materials. The technology relies on microchannels to confine liquid material precursors and promote gelation prior to extrusion, which then occurs by forcing bioinks through a small aperture called spinneret or nozzle. MST offers an increased level of versatility and sophistication compared to other conventional fiber spinning techniques.[3,4]

Biocompatible fibers can be laden with living cells, enabling cell interaction with the surrounding biomaterial, proliferation, and differentiation in a quasi-three-dimensional (3D) environment, superior to two-dimensional (2D) culture systems in terms of biomimicry. However, MST is limited by poor control in spatial arrangement and a lack of macroscopic manufacturing ability. The *in vitro* models obtained result in elongated entangled filaments that fall short of replicating the intricate 3D architecture of native tissues.

Nevertheless, tissue engineering, which aims to create 3D tissues that accurately mimic tissue functionalities[5,6] for regenerative medicine[7,8] and disease modeling purposes,[9,10] has significantly benefitted from the development of MST. As depicted in Figure 1, the strategic incorporation of microfluidic spinning systems on additive manufacturing machines, e.g., 3D bioprinters, fosters the fabrication of advanced spatially-organized *in vitro* models.[11] This coupling via microfluidic operators, such as mixers and filters, enables to control the microarchitecture of fibers, which serve as building blocks for manufacturing functional tridimensional bioconstructs.[12] In this context, research on microfluidics is expanding toward tissue engineering applications, assisting the generation of valuable tools to bioprint functional macrotissues. Conveying the advantages of both techniques, such hybrid strategy allows for the versatile spatiotemporal patterning of fibers as well as the control of multiple bioink deposition for the production of sophisticated 3D structures. The relatively large scale of microchannels diameter (in the range of 100 μm) required to manipulate biomaterial inks—that are thick and often contain living cells—within microfluidic devices allows to benefit from recent innovative microfabrication strategies, which provide valuable alternatives to photolithography, offering higher efficiency albeit in most cases lower resolution.

Starting from recent approaches for microfluidic device fabrication, which now enable to create microdevices in a fast and convenient manner, this review will discuss how the integration of MST is transforming the tissue engineering and regenerative medicine (TERM) field. After presenting general information about desirable biomaterial characteristics and a theoretical model of microfiber formation applicable to most MST strategies, the latest experimental results will be discussed. An insight into current advances both in pure fiber spinning and MST coupling with 3D printing systems (conventional 3D microfluidic bioprinting, c3DMB) is also given. Close attention will be given to monolithic microfluidic platforms, referred to as advanced 3D microfluidic bioprinting (a3DMB) systems.

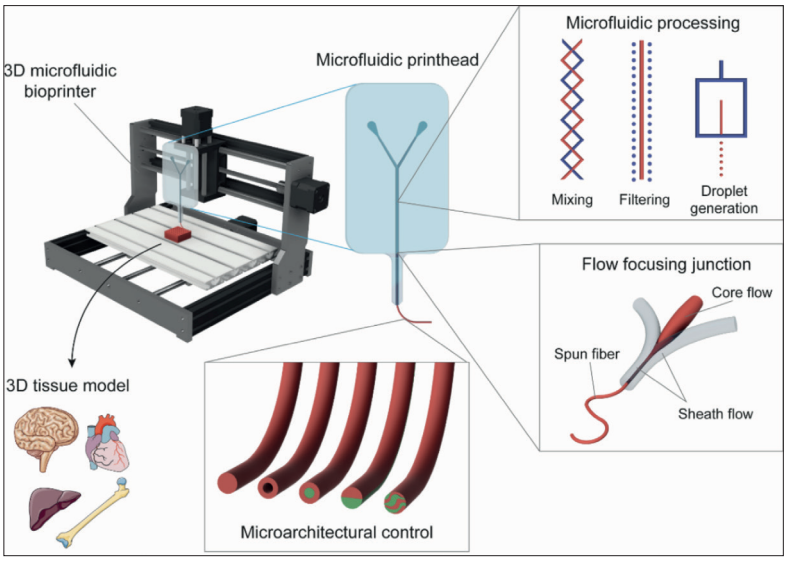

Figure 1. Overview of the microfluidic-assisted 3D bioprinting for the development of functional 3D tissue models. Since laminar flow regime enables fluid handling with extreme accuracy, microfluidic tools allow to perform diverse operations over the bioink, controlling the micromorphology and the functionality of spun fibers to create more reliable in vitro tissue models.

2. Approaches for biomicrofluidic devices fabrication

Microfluidic devices are composed of microchannels with cross-sectional dimensions typically ranging from 0.1 to 1000 μm. The flow regime induced by sub-millimetric confinement is called laminar and implies the predominance of ordered flow patterns, which are only subjected to diffusive mixing at the fluids interface rather than stochastic mixing arising from convective forces.[13,14] In the laminar domain, indeed, flow profiles are deterministic and thus can be mathematically modeled and digitally simulated, allowing to obtain unparalleled level of control over the spatiotemporal dynamics of fluids and molecules.[15,16]

2.1. Traditional microfabrication

Historically, microfluidic devices have been fabricated exploiting microelectronic industry technologies.[17] The simplest way to obtain a microfluidic device consists of generating a master with an embossed pattern that is used to mold polydimethylsiloxane (PDMS). The master mold is fabricated onto a silicon wafer via photolithography with the use of a photomask containing the desired geometry to selectively polymerize a photoresist (typically SU-8 resin), which is previously spin-coated on the substrate. Once the master is available, liquid PDMS is mixed with a crosslinking agent, poured onto the master, and thermally cured. Ultimately, solid PDMS is peeled off, punctured to create access ports to internal structures (i.e., inlets and outlets), and bonded to a substrate (generally glass or PDMS) through air or oxygen plasma treatment[18](Figure 2a).

Although traditional microfluidic manufacturing may achieve elevated resolution (down to the order of 10 nm), the process presents several drawbacks. Photolithography, indeed, is an expensive and time-consuming process[19] and is not accessible to most chemists, biochemists, and biologists. A significant obstacle to adopting photolithography for the quick manufacture of microfluidic devices is the laborious procedure needed to obtain the photomask[20] along with the inability to realize non-planar structures.

2.2. Modern approaches in microfabrication

Leveraging modern approaches such as additive[21] or subtractive[22] manufacturing to fabricate molds for PDMS casting or even entire microfluidic devices has significantly decreased costs and time for producing microfluidic chips. In these cases, a 3D design created through computer-aided design (CAD) software is translated into commands for a computerized numerical control (CNC) machine that builds the 3D object by stacking multiple layers or engraving a bulk piece of material (Figure 2b). The initial geometry, thus, can be digitally modified and immediately re-fabricated, circumventing the tedious procedure of photolithography. Modern microfabrication techniques can produce intricate 3D features and structures with varying heights, which are challenging to achieve with standard photolithography. These innovative strategies enable rapid prototyping complex microfluidic devices and significantly broaden the use of microfluidics among

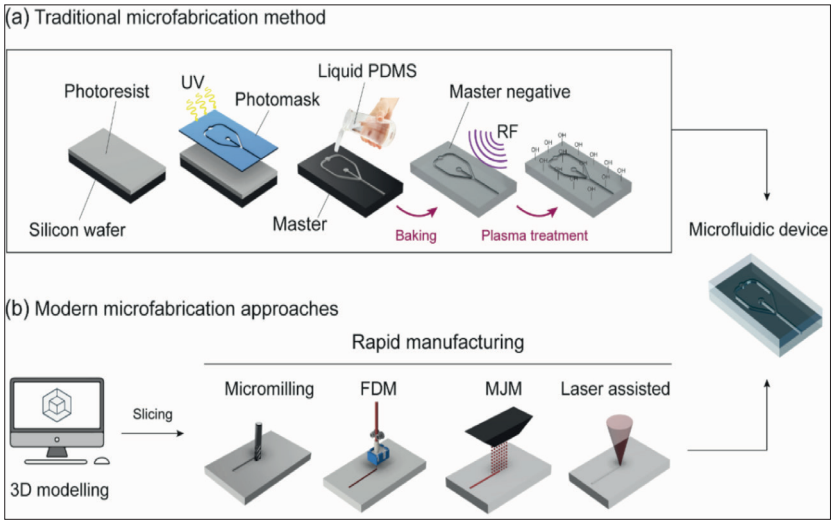

Figure 2. Microfluidic device fabrication. (a) Conventional microfabrication procedure. The master mold for PDMS casting is obtained via photolithography, selectively exposing a photoresist to UV light through a photomask. After casting and thermally curing liquid PDMS against the obtained master, the final device is realized activating PDMS surface to create covalent bonds either with glass or another PDMS slab and realize enclosed channels. (b) Modern microfabrication approaches involve the rapid prototyping of microfluidic devices. Following the design of microchannels geometry with a CAD software, the virtual object is sliced and built via additive or subtractive manufacturing in a faster and more convenient manner.

non-experts. Nowadays, current technologies are starting to replace the gold standard provided by photolithography. Despite the resolution and surface roughness achieved with modern fabrication approaches being often far inferior to the ones obtained via photolithography, these parameters are adequate for most biological-related applications, as the typical dimensions commonly used are in the order of 100 μm.

Moreover, particular care should be taken when handling and cultivating cells on 3D-printed substrates as they may contain a variety of leachates that could impart cell functionality.[23-25] Despite the cytocompatibility issue that reduces the number of available materials, it has been recently shown that PDMS microfluidic devices obtained from 3D-printed molds may successfully support the viable culture of cells, offering a convenient alternative to SU-8 molds.[26]

2.2.1. Micromilling

Milling is a subtractive manufacturing method that relies on machining a bulk piece of material (the *workpiece*) with sub-millimetric precision through a rotating cutting object (the *endmill*). Using a spindle-driven movement along the *Z*-axis and computer-controlled motion in the *XY* plane, a milling system enables the sectioning of fine channels into polymeric transparent surfaces.

Today, micromilling allows for the machining of microchannels with resolution up to 10 μm with an average surface roughness of 2.5 μm[27] that, in addition to the short manufacturing time,[28] makes micromilling a powerful tool for rapid prototyping microfluidic devices with acceptable resolution[29,30] and suitable for bio-related applications. Indeed, several biocompatible materials including hard plastics like polycarbonate (PC), polystyrene (PS), polymethyl methacrylate (PMMA), and cycloolefins (COC or COP) can be machined to obtain master molds or entire microfluidic devices.[28]

At present, the application of micromilling is gradually adopted by the microfluidic community to realize bioinspired platforms and support biomedical research.[31] As a prime example, Costantini *et al*. harnessed milled PC microfluidic devices to build microfluidic printheads for the biofabrication of cell-laden 3D constructs[32-34] while Behroodi *et al*. combined 3D printing and micromilling to realize PDMS devices and produce tumor spheroids.[35]

2.2.2. Extrusion-based technologies

Despite extrusion-based technologies being the most used additive manufacturing approaches to build 3D objects, their use in microfluidic fabrication is quite uncommon. These approaches, which fall under the term of direct ink writing (DIW), construct a microfluidic chip or a stamp to cast PDMS by a layer-by-layer deposition of either single or multiple materials that are processed into fine filaments or tiny droplets. It is possible to divide extrusion-based approaches into two main categories named fused deposition modeling (FDM) and multi-jet modeling (MJM).

In FDM printers, a motorized dispenser nozzle is used to mechanically extrude thermoplastic materials following heating in the form of a filament (in the range between 0.2 and 1 mm[36]) that is rapidly cooled down upon deposition. FDM printers have recently reached the public as they are generally safe, reliable, simple to use, and affordable.[37] However, the fabrication of microfluidic devices harnessing FDM-based approaches has been challenging. The intrinsic structural fragility due to lack of interlayer fusion, the excessive filament size, and the elevated surface roughness (average roughness R_a around 10 μm[38]) of printed pieces hamper the realization of micrometric features with high precision.[39] Interestingly, Zeraatkar *et al*. leveraged the ridges arising from the high roughness of FDM-printed objects to enhance the stochastic mixing of fluids in microfluidic channels.[40] Recently, significant improvements of this manufacturing technique[41] have enabled the engineering of a number of FDM-printed microfluidic devices for bio-related applications[42-45] but not remarkably for fiber spinning purposes. A novel solution for microfluidic manipulation of biomaterials came from the fabrication method proposed by Ching *et al*., who created microfluidic platforms embedding complex operators such as mixers, valves, and droplet generators by directly depositing quick-curing silicone-based resin on diverse transparent substrates.[46,47]

Different from the previous technologies, MJM builds 3D objects by depositing femtoliter droplets onto a tray in a line-by-line, layer-by-layer process. MJM-based 3D printers are equipped with an array of inkjet printheads to allow for multi-material ink deposition. Inks used in MJM printing are typically distinguished in build and support materials, which are deposited in parallel. Besides the ability to perform multi-material, MJM ensures fast printing speed, high precision, and extreme printing quality.[48]

Nevertheless, the high cost of MJM printers as well as the poorly investigated biocompatibility of inks employed represents a huge barrier to the realization of biomicrofluidic devices.[23] Moreover, the removal of the sacrificial material from enclosed structures limits channel dimension to about 200 μm.[49] Some efforts to employ MJM-based printing to fabricate molds[50-53] or entire microfluidic devices[54,55] have been made. As a major example, Sochol *et al*. fabricated complex integrated microfluidic circuits consisting of fluidic capacitors, diodes, and transistors to perform multiple fluidic operations with great accuracy.[56]

2.2.3. Light-assisted technologies

Light-assisted 3D printing comprehends different approaches based on the use of an intense light source, typically in the UV spectrum, to polymerize photosensitive resins composed of functional monomers that join to form polymers after absorbing a sufficient amount of energy.[57]

Stereolithography apparatus (SLA) and digital light processing (DLP) use light to cure the photoresin in a layer-by-layer fashion. While SLA-based approaches exploit a moving mirror galvanometer to deflect the entire light beam in a single spot, a spatial light modulating element (i.e., a digital micromirror device (DMD) or a liquid-crystal display (LCD)) in DLP technology produces a dynamic mask to illuminate each layer entirely, making DLP faster than SLA.[58] Even though optical resolution down to 2 μm is theoretically achieved, the minimum cross-section of an enclosed channel reported is 75 μm.[59] Moreover, the objects manufactured with SLA-DLP technologies exhibit an unparalleled level of surface smoothness compared to FDM and MJM (average roughness, R_a=0.35 μm[38]).

The superior fabrication characteristics of SLA-DLP make this technology the best candidate for the fabrication of entire microfluidic devices or patterned molds. The first attempts to employ laser-based approaches in this field date back between the late 1990s[60] and the first 2000s.[61] Since then, SLA-based technologies have begun to be crucial for the realization of 3D-printed microfluidic chips for a number of applications in the biofabrication field, including fiber spinning.[62-64]

Different from SLA-DLP technologies, direct laser writing (DLW) enables to cure femtoliter volumes of the resin (i.e., 3D voxels) by exploiting the multi-photon polymerization (MPP) process. In this case, a high-intensity and extra-fast pulsed laser (in the order of femtoseconds) is employed. The non-linear absorption of two or more photons causes photopolymerization to occur only in the focus of the laser beam as it is insufficient to polymerize the surrounding regions. This results in the ability to realize feature size down to 100 nm[65] (beyond the diffraction limit) with free-form manufacturing ability and high reproducibility. The high cost of MPP equipment, however, is a significant barrier to the widespread use of this technology.[37,66] Recently, DLW is attracting numerous microfluidic communities to realize chips for the most diverse applications including particle handling[67] and molecular detection.[68] The extreme accuracy in creating sub-micrometric structures is also exploited for realizing complex micro- and nanoarchitectures to mimic intricate biological environments.[66,69,70] Moreover, DLW-based systems have also been harnessed to directly write nanostructures on-chip (in-chip fabrication), enabling the creation of a spinneret with a diameter of 12 μm for spinning microfibers.[71]

3. MST for the production of biocompatible fibers: practical and theoretical aspects

The progress in the fabrication of microfluidic tools remarkably contributed to the creation and advancement of novel biofabrication approaches, fostering the development of increasingly reliable *in vitro* models of human tissues. Thanks to MST technology, microfluidic devices are used not only to confine and culture cells in dedicated 3D platforms (i.e., organ-on-a-chip) but also to fabricate biocompatible fibers homing cells. After extrusion, spun fibers can be either collected in a coagulation bath,[72-75] coiled around a rotating mandrel,[63,76-78] or deposited on a substrate in a predefined shape through a 3D printer (see section 4).

3.1. Approaches and available platforms for fiber formation

MST falls under the umbrella of wet-spinning methods, a wide class of fibers spinning techniques that involves the use of materials in the liquid state to be transformed into solid or gel form after passing through a coagulation bath or a crosslinking solution.[79] In MST, such liquids are confined and manipulated in microchannels.

Various microfluidic solutions have been engineered over the past few decades. Coaxial spinning systems are the most common platforms and are able to produce a coaxial flow of the material precursor and the crosslinking solution, which come into contact at the tip of the spinneret, enabling quick gelation of the gel precursor.[80] Coaxial spinning systems can be realized by arranging two concentric glass capillaries or metallic needles. Also, they can be composed by single[81,82] or multiple capillaries assembled in series to obtain multi-layered flow[75,83,84] as well as coaxial needles combined within a glass tube.[72,73]

In the majority of wet-spinning systems, the phenomenon of hydrodynamic focusing (HF) is exploited to produce coaxial flow and, in turn, fibers. Due to the laminar regime dominating in microchannels, fluids can be manipulated via hydrodynamic focusing by forcing a central fluid stream (*core*)) through a boundary fluid (*sheath*), forming a coaxial flow. Crosslinking agents are included in one of the two solutions, often the sheath fluid, to promote crosslinking and produce compact fibers.[85] Additionally, hydrodynamic focusing not only enables fluid focusing but also acts as a lubricant, enabling the extrusion of the solid fiber. However, to ensure the stability of the whole process, the maintenance of a laminar regime imposes to not have a large difference in core and sheath fluid viscosities.[86] The sheath fluid can be combined with the central one from an angle of 90° or at 45° as it minimally

impacts the central stream diameter or the shear stress created at the fluid interface.[87]

A variety of biocompatible methods for crosslinking fibers in microchannels have been proposed, falling under the categories of light-induced, chemical, and physical gelation. In the former case, fiber hardening is induced by the activation of photosensible species (i.e., photoinitiators) either by ultraviolet (UV) light[63,78,88-91] or by UV-visible radiation.[72,73] Biocompatibility of photoinitiators and light exposure has been assessed for a wide range of mammalian cell types and found to have a minimal impact on cell death.[92,93] Nevertheless, to undergo photopolymerization, biomaterial inks must be functionalized with photosensitive chemical groups (e.g., methacryloyl groups), reducing the range of available materials. In the case of chemical crosslinking, the polymer precursor instantly solidifies when it comes into contact with crosslinking agents such as monomers or enzymes present in the secondary solution.[75,82,84,94] As an example, fibrinogen harnesses the mechanism involved in blood clotting to form fibrin gel when enters into contact with thrombin enzyme.[95] Several mechanisms, instead, are involved in physical crosslinking, including solvent exchange, non-solvent-induced phase separation, solvent evaporation, and ionic interactions. In the latter case, ionically crosslinkable materials (such as alginate) hold the ability to rapidly gel in the presence of ionic species, which intercalate between specific chemical moieties. This method is one of the most popular approaches in biofabrication contexts due to its great simplicity, quickness of gelation, and biocompatibility.[96,97]

The paramount advantage of coaxial wet-spinning methods is the decoupling of printing capability from material rheology,[98] allowing the extrusion even of low-viscosity material blends that include a quick-crosslinkable component (e.g., alginate).[32] Moreover, the method can envision cell encapsulation as the process is entirely biocompatible. Other spinning processes, such as melt- and dry-spinning, are not biocompatible due to the harsh conditions required (e.g., high temperature, toxic solvents, etc.), resulting in the undisputed success of wet-spinning MST-based platforms as novel tools to produce biofibers.[98] Moreover, compared to other spinning techniques employed in the TERM field, such as electrospinning, MST offers superior control over fiber characteristics and internal arrangement of compartments.[99]

3.2. Biomaterial ink design

Biomaterials are designed to simulate the extracellular matrix (ECM) environment in terms of composition, stiffness, and cell adhesiveness. For this reason, naturally-derived components are often the best choice.[100] Commonly, the biomaterial inks are made from: (i) gelatin, a hydrolyzed form of collagen; (ii) alginate, derived from algae; (iii) chitosan, extracted from arthropods' shells; (iv) silk fibroin, a protein found in silk produced by most insects; and (v) fibrinogen, a component of human blood. In certain applications, biomaterial inks are directly derived from the ECM collected from the target tissue, which is ready to host new cells after going through a decellularization process.

The choice of a correct biomaterial is a crucial element for a successful outcome of microfluidic spinning. The achievement of the multi-faceted characteristics desired for the final product[101-103] must be combined with the constraints intrinsically imposed by MST. Indeed, to allow microfluidic manipulations and extrusion from nozzles, materials need to be in the liquid phase[104] and, right after the spinning process, must undergo sol-gel transition to maintain their shape and retain embedded living cells. Common biomaterial inks are based on hydrogels which comprise a solution of high-molecular-weight polymers dissolved in an aqueous solvent. Before crosslinking provides the final rigidity, the polymer chains can slide without constraints relative to each other and the solvent, depending on their chemistry and conformation (e.g., linear vs. branched polymers), conferring the required fluidity to the ink. However, in this state, chain entanglement hinders relative motion under equilibrium; therefore, the material can sustain a certain level of shear stress—the so-called yield stress—before flowing. After the yield stress is exceeded, the entangled chains start sliding, and the material keeps on deforming under shear, like a viscous fluid. The faster the material is sheared, the easier chain sliding occurs as single chains get more and more elongated. As a result, the apparent viscosity of the ink decreases with the shear rate, defined by a rheological behavior called shear thinning (as opposed to shear thickening, a response that is usually of no interest in biofabrication contexts).

3.3. Theoretical model of a biomaterial ink flow in a capillary

The need for microfluidic control and structural features of extruded fibers hence raises the issue of fluid biomaterial rheology modeling. The first thing to consider is that biomaterial inks are far from being Newtonian fluids. Different from elastic solids, for which a stress σ produces a deformation ϵ proportional to the stress itself ($\sigma = M\epsilon$, where M is the elastic modulus), in the simple case of Newtonian fluids, the shear stress produces a liquid flow, according to the equation $\sigma = \eta\dot{\gamma}$. Here, η is the shear viscosity and γ is the relative deformation ($\gamma = \epsilon/L$, with L being the size of the deformed liquid element). This relation implies that for constant σ, the deformation ϵ is

proportional to the time so that there is laminar flow. For the sake of clarity, the quantities σ and ϵ are second-order tensors, while M is a fourth-order one. Here, we refer only to *shear* stress, thus all three quantities are scalar, and the involved modulus is the shear modulus G.

Based on the aforementioned phenomenology, a reliable rheological model of flowing biomaterial inks should combine at least two ingredients, which are:

i) the yield stress, like in a Bingham fluid, which:
   - is rigid ($\dot{\gamma} = 0$) if $\sigma \leq \sigma_0$. Without loss of generality, we assume hereafter that the stress is applied in the positive direction, and therefore, σ is a positive quantity.
   - flows with a viscous stress/shear characteristic $\sigma = \sigma_0 + \eta\dot{\gamma}$ if the yield stress is exceeded.

ii) a shear-thinning response, like in a power-law fluid, with effective viscosity decreasing with the shear rate: $\sigma = \tilde{\eta}(\dot{\gamma})\dot{\gamma}$, where $\tilde{\eta}(\dot{\gamma})$ is the effective viscosity which in turn is expressed as $\tilde{\eta}(\dot{\gamma}) = K\dot{\gamma}^{n-1}$. Here, K is called the consistency index (units in the SI $Pa \cdot s^n$) and n is the power-law exponent ($n < 1$). This combined behavior is well described by the Herschel–Bulkley (HB) model,[105] which for a simple shear flow reads:

$$\dot{\gamma} = \begin{cases} 0, & \sigma \leq \sigma_0 \\ [(\sigma - \sigma_0)/K]^{1/n}, & \sigma > \sigma_0 \end{cases} \quad \text{(I)}$$

If $n < 1$, the viscosity decreases with the shear strength, leading to shear thinning behavior (shear thickening response would be obtained for $n > 1$), as shown in Figure 3a. To summarize, the model parameters are the yield stress σ_0, the exponent $n < 1$, and the consistency index K. Clearly, the HB constitutive relationship is an effective model whose parameters need to be calibrated with experimental data, e.g., acquired with a conical rheometer (Figure 3b).

Although the HB constitutive law should be generalized in the appropriate tensor form to describe a generic flow, the simpler Equation I will suffice here for an introductory illustration of two configurations relevant to biofabrication. Firstly, we consider the flow in a long capillary of radius R_0 under a prescribed pressure gradient $dp/dz|_0$. Momentum conservation

$$\frac{1}{r}\frac{d(r\sigma)}{dr} = \left.\frac{dp}{dz}\right|_0 \quad \text{(II)}$$

demands the force balance $\sigma(r) = 1/2\ dp/dz|_0 r$, where the integration constant vanishes. From the latter, it is clear that the shear stress tends to zero, approaching the capillary axis. This shows that around the axis, $r \leq R_p = 2\sigma_0/dp/dz|_0 r$, a solid region moving rigidly, the rigid plug, should form since the yield stress is not exceeded. From the stress, using Equation I and $\dot{\gamma} = du/dr$, the velocity profile in the capillary can be obtained as:

$$u(r) = \frac{n}{n+1}\left[\frac{1}{2K}\left|\frac{dp}{dz}\right|_0\right]^{1/n} \begin{cases} (R_0 - R_p)^{\frac{n+1}{n}} & r \leq R_p \\ (R_0 - R_p)^{\frac{n+1}{n}} - (r - R_p)^{\frac{n+1}{n}} & R_p < r \leq R_0, \end{cases} \quad \text{(III)}$$

which describes a rigid plug for $r \leq R_p$ and a shear thinning plug ($n < 1$) in the external part of the capillary (Figure 4a).

As a second example, we consider the sheath flow of a Newtonian fluid used to focus the biomaterial in the core of the capillary. Figure 4b shows a HB core and a plug, surrounded by the sheath flow in the annulus $R_0 \leq r \leq R_1$, where R_1 demarcates the boundary between the sheath and the core. The wall viscosity of the HB fluid

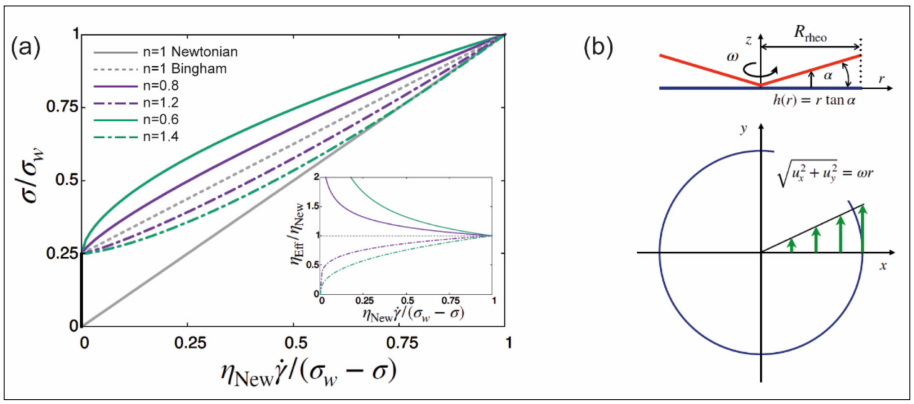

Figure 3.(a) Stress/shear characteristics, σ vs $\dot{\gamma}$, of an HB fluid. The yield stress is set to $\sigma_0 = 0.25\sigma w$, where σ_w is the wall shear stress and η_{New} is the reference viscosity of a Newtonian fluid.In the inset, the effective viscosity η_{Eff} vs $\dot{\gamma}$. (b) Working principle of a conical rheometer. The cone (axial section in red) rotates with angular velocity ω with respect to the base (dark blue). The fluid velocity goes linearly from zero at the base to ωr at the rotating cone, hence the shear is constant $\dot{\gamma} = \omega/tan(\alpha)$.

flowing in the whole capillary without sheath under the given pressure gradient is selected as a reference quantity: $\hat{\eta} = \eta_{Eff}\left(R_0, \frac{dp}{dz}, n\right)$ and the viscosity ratio of HB to sheath fluid is denoted $X = \hat{\eta}/\eta_{sh}$. The sheath flow rate is thus $Q_{sh} = X\hat{Q}_0\,[1 - R_I^{*2}]^2$, with $\hat{Q}_0 = \pi/(8\hat{\eta})|dp/dz|_0 R_0^4$. Hence, $R_I^* = R_I/R_0\sqrt{1-(Q_{sh}/x\hat{Q}_0)^{1/2}}$. The plug is found in the inner region delimited by the radius R_p, with $R_P^* = \frac{R_p}{R_0} = \sigma_0^*$, and the HB flow rate in the core is given by:

$$\frac{Q_{HB}}{\hat{Q}_0} = x\frac{R_I^{*2} - R_I^{*4}}{2} + \frac{n(1-R_P^*)^{\frac{n-1}{n}}(R_I^* - R_P^*)^{\frac{n+1}{n}}}{n+1}\left\{R_I^{*2} - \frac{n(R_I^* - R_P^*)}{2n+1}\left[R_I^* - \frac{n(R_I^* - R_P^*)}{3n+1}\right]\right\} \quad \text{(IV)}$$

The above equations can be used to design the sheath flow: assigning R_I and Q_{Sh} determines the pressure gradient, which in its turn fixes $\sigma_0^* = R_P^*$, the plug region radius, and the overall core flow.

It is worth mentioning that yield stress and shear thinning behavior are not the sole fundamental rheological properties of biomaterial inks. In fact, as with most polymer-based fluids, biomaterials show viscoelastic responses to time-dependent flows.[106] Indeed, due to thermal agitation, polymer chains tend to acquire a coiled state, thus maximizing entropy. When shear is exerted, the chains get elongated, the entropy is reduced, and they react with an elastic force to the external action, leading to a time dependence of the resulting stress.

In elementary terms and neglecting the important effects of chain interactions in dense suspensions,[107] the process takes place on a typical time scale, the (principal) relaxation time τ_R. However, there is another important timescale, τ_F, which measures the typical time of the variation of the applied stress. This could be the period of the oscillation of the stress ($1/\omega$), if the latter is applied at a given frequency $\nu = \omega/2\pi$, or to a sudden change of the condition in the channel, e.g., a fast flow through bents in a micromixer, a sudden stream deflection in a flow-focusing junction, or an abrupt change of shear stress as the extrudate leaves the nozzle. On a general ground, $\tau_F = \sigma/(d\sigma/dt)$. The ratio of relaxation time to flow time scale τ_F defines the Deborah number ($De = \tau_R/\tau_F$), which compares the elastic with the viscous response. The prototypal model of a viscoelastic fluid due to Maxwell[105,108] here written for a simple shear flow

$$\sigma + \tau_R\frac{\partial\sigma}{\partial t} = \eta\dot{\gamma} \quad \text{(V)} \qquad \text{(II)}$$

clearly shows that the behavior is viscous for $\tau_F \gg \tau_R$ ($De \ll 1$) while, to the opposite, it is elastic when $\tau_F \ll \tau_R$, ($De \gg 1$). In fact, Equation V is unsatisfactory in many respects and needs to be generalized in a more complete form, leading to the so-called Oldroyd-B model and a number of other variants,[105] some of which with a direct interpretation in terms of polymer physics.[107,109]

Although the diffusivity of long polymers is low, diffusion effects may be important when different streams meet in a microfluidic mixer or at flow junctions. In addition, surface tension may play a role in extrusion, when the biomaterial ink encounters the external environment (air or suspension medium), while the ink wetting properties on the deposition substrate, as described by Young's contact angle, may be crucial for the actual fabrication process.

Finally, a number of published studies include a far more detailed insight concerning the ink behavior after

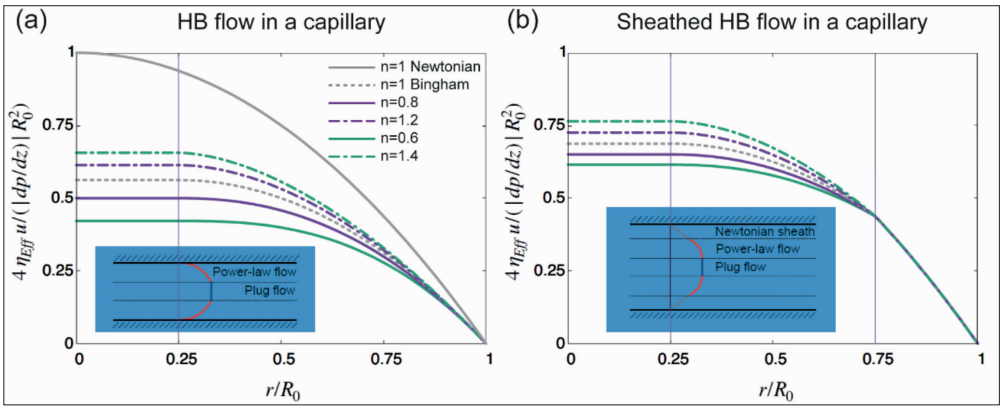

Figure 4.(a) Velocity profiles of an HB flow in a capillary, u vs.r. The plug flow is at $Rp/R_0 = 0.25$ (vertical line). (b) Sheath flow in a capillary: Newtonian sheath ($r/R_0 \geq 0.75$) and HB core ($0.75 \geq r/R_0 \geq 0.25$) with an inner plug flow ($0 \leq r/R_0 \leq 0.25$). The sketches on blue background illustrate the flow structure in the capillary.

crosslinking,[110,111] which determines the final properties of the product, as well as the effect of embedding living cells within biomaterials over ink rheology.[112,113] These subjects are left out of explicit consideration from this section as it aims at describing the spinning of microfibers within microfluidic devices, excluding cell-laden materials.

4. MST for biofabrication purposes

The stunning ability in controlling the composition and compartmentalization of fibers with micrometric precision allows to customize fiber characteristics to build complex quasi-3D environments for living cells that resemble more closely the physiological microstructures[114] (Table 1).

To increase the complexity of spun fibers, additional microfluidic devices can be combined with coaxial needles or glass capillaries to manipulate bioinks before spinning fibers. Microfluidic tools can vary a lot in terms of dimensions, design, and function as they may serve as fluid mixers, splitters, combiners, etc. to create sophisticated patterns along and across the fiber. The precision in handling microflows enables the continuous and controlled formation of fine filaments with a wide range of structural and functional properties.[88,115-117] Indeed, fluids can be prior combined within the microchannels and then extruded as uniform,[118] hollow,[119,120] core-shell,[121,122] or heterogeneous (i.e., Janus)[33,123,124] filaments. In the case of multi-material deposition, microfluidic systems can provide seamless transitions between biomaterial inks harnessing valves[125,126] or flow withdrawal.[127] On the other hand, progressive and controlled variation of material composition is often sought to replicate the intricate *in vivo* environment, especially in tissue interface portions.[128] Functionally graded structures can be obtained by adding a microfluidic mixer to the system that allows to gradually modify fiber composition to create mechanical, chemical, or cellular gradients. Alternatively, microfluidic operators can be used to generate and pattern monodispersed bubbles containing cells or functional agents inside the fibers.[129,130]

4.1. Fiber production via MST: building quasi-3D environments

One of the first pioneers in this field was Kim *et al.*, who in 2008 spun chondrocytes-laden alginate fibers in a $CaCl_2$ bath[131] harnessing a flow-focusing PDMS chip dipped in the crosslinking solution. Although rudimentary equipment was used, the basic principles are still used today for spinning cell-laden fibers. Evidently, more complex fiber profiles can be generated thanks to the fluid linearity in microchannels. In particular, by allowing two or more fluids to flow aside and fixing through crosslinking, hybrid and multi-compartment fibers can be produced.[117,132] Alternatively, integrating a flow-focusing junction upstream, the central compartment can be sheathed by a second fluid before crosslinking to form a core-shell flow profile.[91] To integrate all these elements, Guimarães *et al.* developed a unique microfluidic chip based on a flow-focusing geometry for the production of (i) multi-compartment, (ii) core-shell, (iii) hollow, and (iv) fibers containing oil droplets for the creation of complex biological micromodels[3] (Figure 5a). As a unique example, core-shell gelatin methacryloyl (GelMA) fibers with straight and helical morphologies embedded in an alginate shell have been fabricated harnessing the coflow rope-coil effect[73] (Figure 5b). In the case of hollow fibers generation, a sacrificial material is flowed in the core and then dissolved to leave an empty cavity for nutrient delivery. This technique is widely used to simulate microvasculature environment[81,133] or to guide the vascularization of fiber-shaped tissues,[83] which is a crucial aspect in biofabrication contexts.[134]

A remarkable example of accurate fabrication of multi-compartment and multi-hollow fibers is provided by Cheng *et al.* who designed a device made of aligned scalable multi-barrel capillaries to fabricate microheterogeneous fibers in one step. As shown in Figure 5c, Janus and multi-shell hollow alginate fibers of 40–120 μm in diameter were formed.[135] In a further study, the authors demonstrated the possibility to create anisotropic fibers with two or three compartments, which can be independently provided with a single or double hollow core[136] (Figure 5d and e). A similar approach has been proposed by Yu *et al.* where a PDMS chip was employed to fabricate multiple hollows (up to five cavities) and multi-compartment fibers with extreme control[74] (Figure 5f).

When spinning cell-laden fibers, morphological and mechanical cues are fundamental for functional cell development. MST allows to generate fibers with diverse cross-section[99,137] to provide morphological guidance for cell proliferation. Specifically, it has been demonstrated that the formation of grooves on the surface of fibers contributes to improved directional alignment of cultured cells.[88,90,138] Alternatively, extruded fibers can be mechanically stimulated by stretching either when collected around a rotating tool by adjusting the intensity of pulling or after printing. As an example, Rinoldi *et al.* exploited a rotating mandrel to collect fibers laden with human bone marrow stromal cells (hBMSCs) followed by mechanical and biochemical stimulation for tendon regeneration purposes.[78] The authors showed how static stretching of fibers before culture, along with biochemical stimulation, leads to enhanced expression of tendon target genes. Likewise, Costantini *et al.* exploited a similar version of the aforementioned microfluidic system, in which the coaxial needle is replaced with a milled PC

Table 1. Summary of different technologies used to produce biocompatible fibers, even cell-laden, presenting different morphologies and material compositions that are produced with capillary microfluidic platforms or with a microfluidic chip

Spinning technology	Spinning platform	Fiber type	Material	Crosslinking agent	Cell type	*In vivo*	Ref.
Capillary microfluidics (glass or metallic connectors)	Glass capillary	Solid and peapod-like	Chitosan/Polyethylene glycol (PEG)	GTA	/	/	[94]
		Solid	PEG with maleimide end groups (PEG-4Mal)	DTT + TEA	NIH 3T3, MC3T3	No	[82]
		Multi-compartment, hollow and combination	Alginate	$CaCl_2$	/	/	[135]
		Hollow	Alginate/GelMA	$CaCl_2$ + LAP (UV-Vis)	HUVECs, MC3T3-E1	No	[81]
		Hollow	Chitosan/Gelatin	TPP	NIH 3T3	No	[133]
	Metallic needle in a glass capillary	Hollow	Gelatin/GelMA	LAP (UV-Vis) in ice bath	HUVECs	No	[72]
	Coaxial nozzle in glass capillary	Solid straight and spiral	Alginate/GelMA	$CaCl_2$ + LAP (UV-Vis)	HUVECs	No	[73]
	Glass capillary + rotating motor	Core-shell	Alginate/Collagen/ Fibrinogen	$CaCl_2$	NIH 3T3, C2C12, Cardiomyocytes, HUVEC, MS1, Nerve cell Cortical cells, Neural stem cells, HepG2, MIN6m9, HeLa	Yes	[83]
	Coaxial needles + rotating motor	Solid	Alginate/GelMA	$CaCl_2$ + Irgacure (UV)	hBM-MSCs	No	[78]
	Triple-orifice coaxial needles	Solid, hollow, core-shell	Gelatin–hydroxyphenylpropionic acid (Gtn-HPA)	HRP/H_2O_2	MDCK, NIH 3T3	No	[75]
		Solid, hollow, core-shell	Gtn-HPA, NIPAAM, Alginate	HRP/H_2O_2 + $CaCl_2$	/	/	[84]
Microfluidic devices (without glass or metallic connectors)	PDMS chip	Solid, hollow, with oil droplets	Gellan gum	$CaCl_2$	/	/	[3]
		From thin flat to cylindrical	Alginate	$CaCl_2$ in IPA	/	/	[203]
		Multi-compartment and multi-hollows	Alginate/PVA	$CaCl_2$	/	/	[74]
		Solid	Alginate	$CaCl_2$	/	Yes	[204]
		Multi-compartment	Alginate	$CaCl_2$	NCI-H1650, HUVECs, HFL1	No	[132]
		Core-shell with micropassage	Alginate/PGA	$BaCl_2$	NIH 3T3 and A549	No	[205]
		Solid	Alginate/PEGDA	$CaCl_2$ + Irgacure (UV)	/	/	[89]
	PDMS chip + rotating motor	Flat stripe-patterned	Alginate/PGA	$BaCl_2$	HepG2, Swiss 3T3	No	[117]
		Grooved	Alginate/GelMA	$CaCl_2$ + Irgacure (UV)	C2C12	No	[88]
	Syringe and PDMS chip	Solid, Solid patterned	GelMA	Irgacure (UV)	C2C12	No	[90]
	PC chip + rotating motor	Solid	PEG-fibrinogen/ alginate	$CaCl_2$ + Irgacure (UV) + thrombin	nLacZ- (Mabs)	Yes	[63]
	PMMA/COC chip	Solid, hollow, core-shell, multiple core-shell	PEGDMA/ GelMA	Irgacure (UV)	/	/	[91]
	Biocompatible resin	Core-shell with different core materials	Fibrinogen, alginate	$CaCl_2$	C2C12	No	[139]

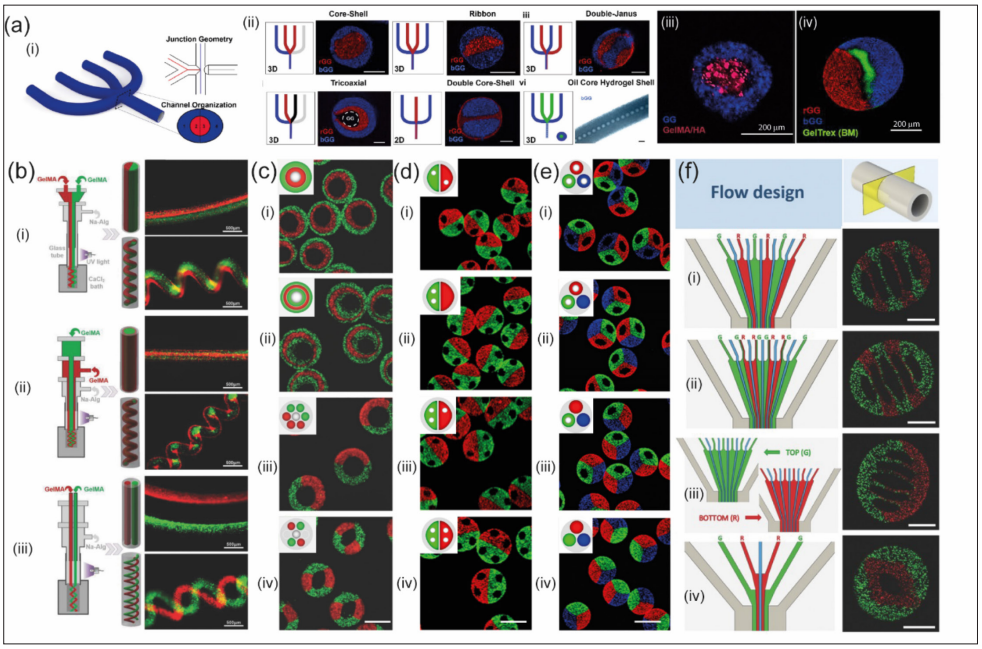

Figure 5.Microfluidic spinning of complex functional fibers. (a) Multi-functional 3D flow focusing microfluidic chip. (i) Sketch of the microfluidic channel geometry, (ii) different flow configurations of the flow focusing device (scale bars are 100 µm) to produce (iii) core-shell fibers for vasculature, and (iv) ribbon fibers for modeling cancer/BM/stroma environment. Adapted with permission from.[3] Copyright © 2021, Elsevier. (b) Generation of multi-compartmental straight and helical GelMA microfibers with (i) Janus, (ii) core-shell, and (iii) double core structure. Adapted with permission from.[73] Copyright © 2018, Wiley-VCH. (c) Janus and multi-shell hollow alginate fibers with (i) two shells, (ii) three alternate shells, (iii) two-compartment shell, and (iv) four-compartment shell. Scale bar is 200 µm. Adapted with permission from.[135] Copyright © 2014, Wiley-VCH. (d) Fibers with two compartments that can be independently provided with a single or a double cavity. Scale bar is 200 µm.Adapted with permission from.[115] Copyright © 2016, American Chemical Society. (e) Fibers with three compartments that can be independently provided with a hollow. Scale bar is 200 µm. Adapted with permission from.[115] Copyright © 2016, American Chemical Society. (f) Production of multi-hollow (up to fivecavities) and multi-compartment fibers. (i) Fiber with six compartments and five hollows, (ii) fiber with five compartments and five hollows, (iii) fiber with two compartments and five hollows, (iv) fiber with double shell and a single hollow. Scale bars are 100 µm. Adapted with permission from.[74] Copyright © 2016, Wiley-VCH.

nozzle, to fabricate myosubstitutes with high throughput and functionality.[63] The authors highlighted how the mechanical pulling of fibers during the extrusion phase created highly anisotropic fibers that better replicate the aligned microarchitecture of myotubes. As a result, both *in vitro* and *in vivo* myobundle creation and muscle cell precursor differentiation were enhanced. Recently, the same microfluidic spinning system has been further improved and the PC tool has been replaced with a 3D-printed nozzle, which is fully immersed in a $CaCl_2$ bath.[139] As the bioink reaches the tip, it is immediately crosslinked and wrapped around an automatized rolling rod where annular fiber bundles are collected. Core-shell fibers with different core materials have been successfully produced, maintaining a highly-aligned cell distribution. The authors demonstrated that different mechanical and electrical stimulation of the muscle constructs post-extrusion modifies the expression of key marker proteins of neo-forming myotubes.

Despite the great advantages conveyed by the coupling of microfluidics and coaxial extrusion methods, technical limits related to the system integration restrict the potential and fineness of the strategy. In fact, since microfluidic modules and coaxial extruder are connected manually, flow perturbations may arise from the geometrical discontinuity at the junction between the microfluidic channel and the dispensing needle, compromising the pattern created upstream and the final resolution of the printed scaffolds. Owing to leaks at the final connection, users are frequently forced to repair or replace the dispensing system after or even during the printing process. Additional drawbacks arise from inherent limitations of the coaxial wet-spinning method, including the high shear stress levels generated inside the needle[140] and the inability to control fiber diameter on-chip in real time. The manual preparation of the nozzles also leads to limited replicability and poor coaxiality of the flow, often impairing the accuracy of the extrusion process. To limit these issues, monolithic microfluidic chips can be harnessed to produce fibers without requiring any additional components rather than engraved microchannels. Such devices, either realized with conventional lithography or via 3D manufacturing strategies, provide higher ease and repeatability of realization, representing a valuable alternative to conventional microfluidic coaxial wet-spinning platforms.

4.2. Coupling MST with 3D bioprinting: building 3D constructs

Spun fibers alone cannot replicate the hierarchical 3D architecture found in human tissues, limiting the use of *in vitro* models to the fabrication of elongated structures such as blood microvessels[141] and kidney proximal tubules.[142] 3D bioprinting has lately come to the fore as a revolutionary technology for biofabrication. Contrary to mere MST, the combination of MST with 3D printing enables the precise control of the arrangement of fibers into predetermined 3D shapes. This allows for the creation of heterogeneous and anisotropic constructs that more closely resemble the complexity of the *in vivo* environment and ultimately impart the desired tissue functionality.

4.2.1. 3D bioprinting

Analogous to 3D printing platforms, 3D bioprinters enable the deposit of bioinks (material inks comprising living cells) to fabricate 3D *living* constructs. In the context of biofabrication, 3D bioprinting platforms comprise laser-assisted,[143-146] inkjet,[147-149] and extrusion-based systems to generate viable and functional tissue substitutes. In this review, we are focusing on MST integration in bioprinting systems, typically in extrusion-based machines, where bioinks are processed into complex filaments before being extruded. However, it is worth mentioning that Wang *et al.* have recently demonstrated the possibility to integrate a microfluidic mixer with a DLP-based fabrication system to create multi-functional 3D gradients.[144]

Custom-made 3D bioprinting systems are commonly realized by combining computerized driving of the nozzle in the *XYZ* direction with a pumping apparatus, which can be either air-, piston-, or screw-driven, to perform robotic dispensing of biomaterials. The extruded fiber represents the building block of the ultimate 3D-printed construct, and fiber diameter (in the sub-millimetric range) provides the final resolution. A 3D bioprinter can be equipped with different tools acting as printing heads, which can be either simple syringes with a needle, coaxial nozzles made from glass capillaries or metallic needles, microfluidic devices with coaxial nozzles or monolithic PDMS chips (Figure 6, Table 2).

In the simplest case, since shear-thinning materials can retain their shape after extrusion, they can be directly extruded from a syringe and deposited onto a substrate[150] (Figure 6a). This approach, called DIW, is sometimes coupled with photocuring[151-157] and, owing to its simplicity, undoubtedly represents the most widely used biofabrication method. In the case of extremely low-viscosity biomaterial inks, free-form 3D objects can be printed inside a supporting bath to retain the target shape and subsequently crosslinked to enable the removal of the construct from the embedding medium.[158-160] Alternatively, ionic crosslinking represents a valid and widespread solution, enabling to solidify and extrude the bioink using a coagulation bath[161] or coaxial wet-spinning systems.[162]

Recently, a new approach is emerging in the biofabrication panorama, consisting of the creation of handled platforms to spin cell-laden fibers directly in the site of interest.[163-166] This innovative solution, which takes the name of *in situ* bioprinting, has a large number of advantages compared to the other methods including its printing versatility and ease of use. Moreover, *in situ* bioprinting minimizes the manipulation of printed constructs, avoiding the risk of damage or contamination, and allows the body itself to act as a bioreactor, creating the optimal conditions for physiological tissue regeneration.

4.2.2. Coaxial wet-spinning 3D bioprinting

Coaxial wet-spinning 3D bioprinting relies on fiber deposition through a coaxial nozzle that is driven in the 3D space thanks to the movement of the 3D printing machine (Figure 6b). Due to the easy and low-cost fabrication, coaxial needles or capillaries can be assembled in a variety of configurations to spin uniform,[162,167] hierarchical (e.g., core-shell, spindle-knot), multi-component fibers, or combinations of them.[168]

In the frame of vascular tissue engineering, hollow fibers can be produced by flowing the crosslinking solution or a fugitive material (e.g., polyvinyl alcohol [PVA], Pluronic F-127) in the core compartment.[169-171] Gao *et al.* demonstrated the possibility to use a coaxial needle to deposit hollow fibers within a coagulation bath, obtaining lattice, cylindrical, and thick cubic structures.[169] In a further study, the same group built a system to create a 3D vessel-like structure by extruding a fiber and wrapping it around a rotating rod.[172] Fibroblasts and smooth muscle cells are embedded in the spun fiber, while endothelial cells are subsequently seeded in the lumen of the cylinder. In this way, the authors were able to create a vascular tube that has been ultimately proven to support internal flow. As another example, Pi *et al.* presented another promising multi-channel coaxial extrusion system harnessed to 3D-print hollow filaments, which recapitulate circumferentially multi-layered tubular tissues such as blood vessels and urethra. This approach also enabled the fabrication of continuous fibers alternating single and multi-layered cross-section[121] (Figure 7a). In 2022, Wang *et al.* demonstrated the possibility to bioprint functional acellular hollow conduits, recreating the structure of veins and arteries.[173] Specifically, to obtain fibers with internal lumen, the $CaCl_2$ solution was flown in the core compartment while a single or two types of materials were flowed in the sheath compartment. Smooth muscle cells, either derived from veins or arteries, were seeded on top

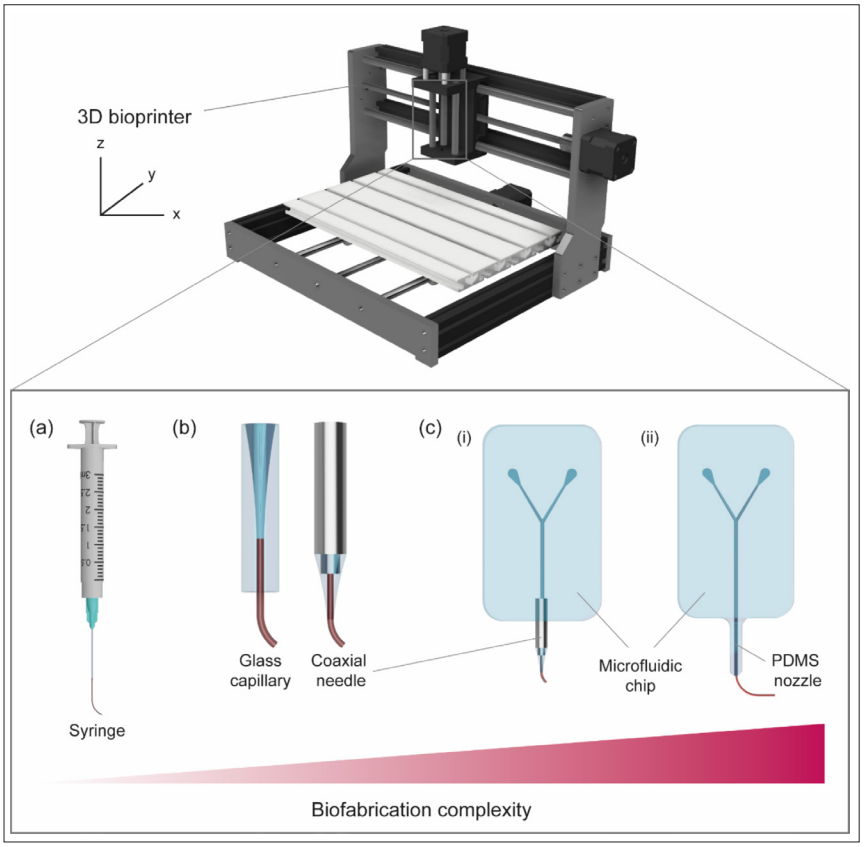

Figure 6.Types of 3D bioprinting extruders. (a) In DIW approaches, a syringe is used to extrude a biomaterial or a bioink directly onto the substrate. (b) Coaxial needles and glass capillaries are used in coaxial wet-spinning bioprinting to quickly solidify a material precursor with a crosslinking sheath solution coming from the outer shell. (c) Upstream the coaxial needle, the integration of a microfluidic chip enables the creation of more complex patterns within the fiber. The microfluidic printhead can be provided with (i) a metallic connector or a glass capillary (c3DMB) or with (ii) a PDMS nozzle (a3DMB).

Table 2. Diverse approaches for 3D biofabrication of functional fiber-based 3D in vitro models

Bioprinting approach	Biomaterial	Crosslinker	Fiber type	Cell type	Application	Ref.
Coaxial wet-spinning 3D bioprinting	Alginate/GelMA/PEG-DA, Pluronic F127	$CaCl_2$, Irgacure 2959	Hollow	VSMCs	Vasculature	[206]
	GelMA, chondroitin sulfate amino ethyl methacrylate (CS-AE-MA), hyaluronic acid methacrylate (HAMA)	$CaCl_2$, Irgacure 2959	Solid	hBM-MSCs	Cartilage	[32]
	GelMA, alginate, PEGOA	Irgacure 2959	Hollow multi-layered	C2C12, NIH-3T3, HUCs, BdSMCs, hSMC, HUVECs	Urothelial tissue, Vasculature	[121]
	Alginate, chitosan	$CaCl_2$, EDC, Genipin	Solid	HepaRG	Hepatic tissue	[162]
	Alginate, Matrigel	$CaCl_2$	Solid	iPSCs	Neural tissue	[167]
	Alginate, GelMA, PVA	$CaCl_2$	Solid, core-shell, multi-core, multi-layered, Janus, spin-dle-knotted, structured	/	Multi-functional and tailorable fibers	[168]
	Alginate	$CaCl_2$, $CaCl_2$ bath	Hollow	L929	Nutrient delivery	[169]

Continued

Table 2. *(Continued)*

Coaxial wet-spinning 3D bioprinting	Vascular-derived ECM (VdECM), alginate, Pluronic F127	Ca^{2+} ions in Pluronic F127	Hollow	HUVECs, hAECs, HL-60	Vasculature	[170]
	Alginate, GelMA, SilkMA	$CaCl_2$, Irgacure 2959	Hollow	HUVECs	Vasculature	[171]
	Alginate, methylcellulose, gelatin	$CaCO_3$, GDL	Hollow multi-layered	MG-63	Vasculature	[174]
	Alginate, GelMA	$CaCl_2$ bath, Irgacure 2959	Hollow multi-layered	MG-63, HUVECs	Vasculature	[175]
	Alginate	$CaCl_2$, citrate buffer	Hollow branched	Mouse fibroblasts	Vasculature	[176]
	Alginate, gelatin	$CaCl_2$, mTG	Hollow mono- and dual-layered	HUVECs, HUAECs, HUVSMCs, HUASMCs	Vasculature	[173]
Conventional 3D microfluidic bioprinting (c3DMB)	Alginate, PEG-Fibrinogen	$CaCl_2$, Irgacure 2959	Janus	C2C12, BALB/3T3	Muscular tissue	[33]
	GelMA, CS-AEMA, HAMA, alginate	$CaCl_2$, Irgacure 2959	Solid	hBMSCs, hACs	Cartilage tissue	[34]
	PVA, PAN, TPU	PEG, PEO	Solid	/	Textile industry	[118]
	Alginate	$CaCl_2$	Hollow	*Escherichia coli*, K12, HUVECs	Vasculature	[119]
	AlgMA, hyaluronic acid (HA)	$CaCl_2$, Irgacure 2959	Solid, hollow, hollow multi-layered	MG-63, HUVECs	Vasculature	[120]
	Alginate, GelMA	$CaCl_2$, Irgacure 2959	Solid, Janus	HUVECs, cardiomyocytes	Cardiac, muscular	[123]
	Alginate	$CaCl_2$ in agarose	Solid, Janus	HUVECs, H9C2	Multi-cellular	[124]
	Carboxymethyl chitosan (CMCh), hyaluronic acid oxide (HAox), HA	/	Solid	L929	Multi-functional 3D hydrogel fabrication	[177]
	Alginate	$CaCl_2$ bath	Solid chaotic	*E. coli*	Polybacterial microsystems, tissue-microbiota models	[178]
	Alginate, graphite, GelMA, PEO	$CaCl_2$ bath, LAP	Solid chaotic	*E. coli*, C2C12	Multi-scale layered biological structures	[178]
	Alginate, GelMA	$CaCl_2$, Irgacure 2959	Solid chaotic	C2C12	Muscular tissue, biotextile	[179]
	Agarose	$CaCl_2$	Solid graded	HEK-293	Gradients fabrication	[182]
Advanced 3D microfluidic bioprinting (a3DMB)	Alginate	$CaCl_2$	Solid	/	3D hydrogel fabrication	[184]
	Fibrinogen, alginate	$CaCl_2$, chitosan, genipin, thrombin	Solid	hiPSCs[160], MSCs[162], U87MG[163]	Neural tissue[160,162], GBM model[190]	[185,189,190]
	Fibrinogen, alginate, PVA	$CaCl_2$, chitosan, genipin, thrombin	Solid with PVA microspheres	hiPSCs	Neural tissue	[192]
	Alginate, collagen type I, dECM	$CaCl_2$	Solid	HASM, HISM	Smooth muscle tissue	[194]
	Alginate, gelatin, pectin	$CaCl_2$	Core-shell	pmTECs, HUVECs	Kidney tissue	[195]
	Alginate, collagen type I	$CaCl_2$	Multi-material, mixed, solid, with controlled cell density	NOR-10 fibroblasts	Multi-functional[169], cell density control[170]	[196,197]

of the fibers, while endothelial cells were perfused within the lumen. Eventually, the formation of a functional and sealed conduit was confirmed by the expression of specific target genes and perfusion tests (Figure 7b). By creating a triple coaxial flow of different materials, it is also possible to generate more complex fibers, such as tri-layered core-shell fibers[174,175] or branched microfibers.[176]

4.3. 3D microfluidic bioprinting: enhancing the complexity of 3D constructs

The use of low-viscosity inks has conveyed manifold advantages, among which the possibility to process hydrogel precursors within microfluidic channels before extrusion (Figure 6c). Coupling microfluidic operators upstream of the extrusion printhead enables the 3D manufacturing of complex scaffolds tailored to their micro-

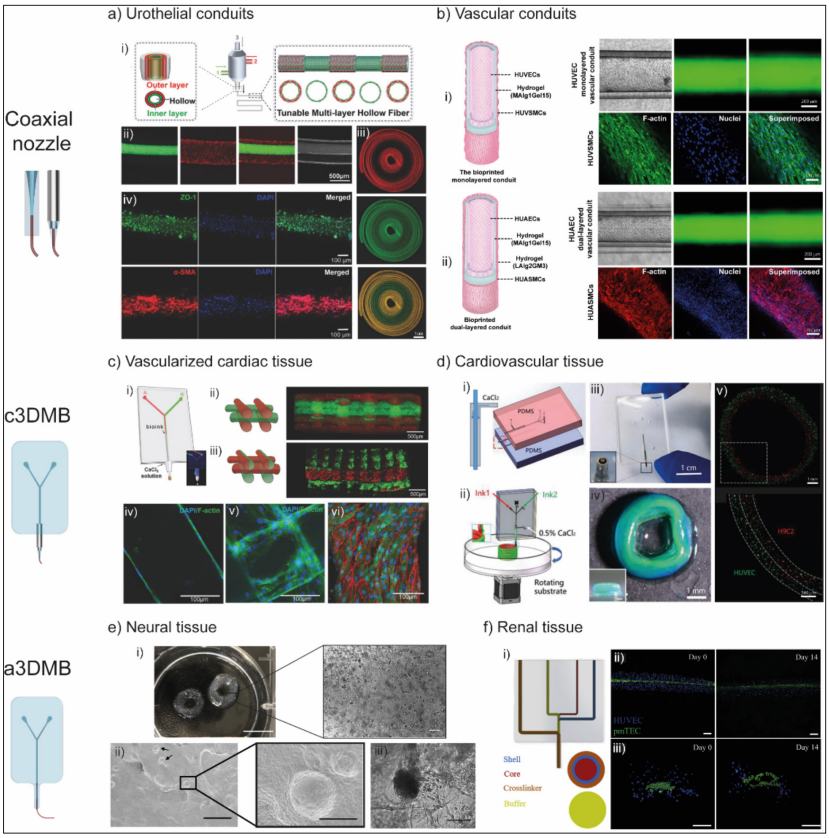

Figure 7.Microfluidic spinning platforms and 3D-bioprinted models.(a) Fabrication of perfusable double-layered fiber-based 3D constructs. (i) Sketch of the coaxial nozzle system and the extruded fiber alternating single and double-layered regions, (ii) fluorescence microscopy images of double-layered hollow fibers, (iii) printed spiral structures showing dynamic change between single and double-layered fiber morphology, and (iv) expression of characteristic urethral biomarkers at day 14 revealed by confocal microscopy images of immunostained urothelial conduits. Adapted with permission from.[121] Copyright © 2018, Wiley-VCH.(b) 3D bioprinting of functional and tough vascular conduits through a coaxial needle system. (i) Recreation of a vein-like tissue based on mono-layered hollow fibers laden with veins-derived endothelial and smooth muscle cells. (ii) Recreation of an artery-like tissue based on double-layered hollow fibers laden with artery-derived endothelial and smooth muscle cells. In both cases, FITC-dextran diffusion and expression of target protein confirms the formation of a sealed and functional vascular conduit. Adapted with permission from.[173] Copyright © 2022, AAAS.(c) 3D microfluidic bioprinting of multi-compartment fibers. (i) Illustration of the microfluidic chip, (ii) printing of a scaffold with alternate layers, (iii) printing of a scaffold with alternate layers and hybrid fibers, (iv, v) Confocal microscopy images of fiber cross-section and top view showing cell migration towards the outer fiber surface. (vii) Top view of a single cell laden fiber immunostained for CD31 and DAPI. Reproduced with permission from.[123] Copyright © 2015, Wiley-VCH.(d) Printing of multi-cellular constructs through a c3DMB based system harnessing a rotating substrate. (i) Structure of the microfluidic device, (ii) sketch of the 3D bioprinting procedure, (iii) macrograph of the final microfluidic device, with focus on the coaxial needle, (iv) photograph of the 3D-printed ring construct, (v) fluorescence image of a 3D-printed ring construct containing HUVECs and H9C2 on the external and internal parts, respectively. Reproduced with permission from.[124] Copyright © 2019, Feng et al.(e) Monolithic microfluidic printhead for high density cellular printing.(i) 3D-bioprinted ring structures at day 0 and enlarged view. Scale bars are 10 mm and 100 µm, respectively. (ii) SEM imaging at different magnifications of spheroids bulging from the fiber at day 3.Scale bars are 50 µm and 100 µm, respectively. (iii) SEM image of a single spheroid bulging from a fiber at day 12. Scale bar is 100 µm.Reproduced with permission from.[191] Copyright © 2018, Elsevier.(f) Development of a functional renal in vitro model through a3DMB. (i) Illustration of the microchannel geometry within the microfluidic device and scheme of the fiber cross-section. (ii) Top view of core-shell bioprinted fibers laden with HUVECs and pmTEC at day 0 and day 14. (iii) Cross-sectional view of core-shell fibers showing the formation of a hollow conduit after 14 days of culture. All scale bars are 200 µm. Adapted with permission from.[196] Copyright © 2020, Elsevier.

and macromorphology.[11] In this review, the strategies employed to pair microfluidics and 3D bioprinting are divided into two categories: (i) conventional microfluidic 3D bioprinting (c3DMB), which relies on the connection of a microfluidic device to a conventional coaxial wet-spinning system, and (ii) advanced 3D microfluidic bioprinting (a3DMB) that implements the sole microfluidic chip with an inbuilt PDMS coaxial nozzle to pattern and spin fibers.

4.3.1. Conventional 3D microfluidic bioprinting (c3DMB)

One of the most representative examples of the integration of a microfluidic device with the coaxial wet-spinning method has been developed by Colosi *et al.* in 2016.[123] The proposed system consisted of a microfluidic platform comprising separated inlets where two biomaterials flow and eventually converge into a single channel connected to the internal needle of a coaxial system. The processed biomaterial ink is then solidified through a $CaCl_2$ solution flushing in the outer shell. Despite its simplicity, this spinning platform has been employed to fabricate micro-compartmentalized fibers with configurable composition, offering great potential for cardiovascular applications[33] (Figure 7c). A new system for multi-material deposition was proposed by Feng *et al.* in 2019, a Y-shaped PDMS microfluidic chip mounted on a rotating motor coupled to a simple metallic nozzle or a coaxial needle.[124] To retain the same heterogeneous morphology of the alginate-based filaments across the layers, path variations are matched with chip rotation. In addition, multi-cellular concentric rings including human umbilical vein endothelial cells (HUVECs) and H9C2 myoblasts were fabricated by depositing the Janus fiber on a rotating substrate (Figure 7d).

Despite achieving efficient mixing is challenging in microfluidic devices, new passive micromixers have been recently designed to tune the microtopography of the section of the fiber and control cellular arrangement. In last years, the Kenics-type static mixer geometry has been established as a gold standard to spin complex heterogeneous fibers made up of two or more components.[177-179] In fact, a series of helical Kenics elements can passively produce chaotic mixing in a few millimeters with high efficiency. Samandari *et al.* realized a 3D microfluidic chip to create multi-compartmentalized hydrogel fibers with micro- and nanometric control and showed how fiber microarchitecture affects cell proliferation and differentiation.[180] Specifically, mixed filaments of alginate and GelMA are obtained by harnessing up to 7 helical Kenics elements, then extruded through a coaxial needle with a $CaCl_2$ solution, and subsequently crosslinked with UV light.

To replicate the gradual variation of physical and morphological properties present in human tissues, microfluidic mixers are devised to deposit fibers that are uniform across the cross-section and gradually vary along the fiber length.[181,182] One notable example is provided by Idaszek *et al.*, who adopted micromilling technology to engrave a micromixer into a thick polycarbonate sheet.[34] By regulating the two bioink flowrates and progressively switching between them, a continuous axial gradient is created. A coaxial extruder is positioned downstream of the microfluidic device to enable continuous manufacturing of thin fibers using $CaCl_2$ as the crosslinking solution. With the use of two bioinks specifically formulated to resemble the native ECM and laden with human articular chondrocytes and hBMSCs, it was feasible to replicate the interface between hyaline and calcified cartilage. Another strategy has been proposed by Kuzucu *et al.*, in which two syringe pumps are connected to a mixing unit placed right before the extruder. In this instance, both planar (2D) and axial (3D) gradients in terms of stiffness, peptide, and cell concentration have been successfully realized.[183]

c3DMB has been extensively harnessed to print hollow fibers for the creation of vascular microchannels, enabling tissue vascularization.[120,171,175] Attalla *et al.* devised a multi-axial extrusion system by connecting a winding hollow channel made in PDMS to embedded needles with increasing size, enabling the formation of bi-[119] and tri-axial[184] flow. Fibers with concentric layers housing endothelial cells and fibroblasts were generated by blending alginate with collagen and fibrin.

4.3.2. Advanced 3D microfluidic bioprinting (a3DMB)

Even though the majority of efforts have focused on the coupling of microfluidic tools with traditional metallic nozzles, recent studies have also demonstrated the possibility to realize an entirely-microfluidic printhead.[185,186] Following this strategy, the conventional coaxial wet-spinning system is replaced by a flow-focusing-based chip, which operates as the actual printhead moving in the 3D space while depositing the fiber.

The core-sheath flow profile generated enables fast solidification of material precursor, via either ionic crosslinking or fast chemical reactions.[186] a3DMB platforms allow to tailor the ultimate fiber diameter in real-time and on-chip by adjusting the relative flow rate of core and sheath components,[187] ultimately achieving a range of fiber diameters much wider than the one obtained with c3DMB. In fact, in the latter case, the insertion of physical constraints (e.g., metallic connectors, glass capillaries) binds the fiber dimension and only the printing speed can modulate the effective fiber diameter. Moreover, as

highlighted in the theoretical model, the introduction of a sheath flow protects encapsulated cells from harsh spinning conditions,[188] minimizing the level of shear stress imparted to the central stream, thus enabling the successful printing of high cell density bioinks. Adopting this strategy, the microfluidic extruder and the upstream microfluidic modules can be connected through flexible tubes or even integrated into a single platform, minimizing flow perturbations and dead volumes.

In 2013, Beyer *et al.* presented the first connector-free microfluidic device employed as a printhead to fabricate and deposit alginate fibers with diameters ranging from 75 to 300 μm with a calcium chloride sheath flow.[185] Moreover, the prototype was incorporated with pneumatic valves to perform accurate switching between different bioinks.[189] Extruded fibers were deposited into simple 3D structures (ring-shaped or cuboid) onto a porous substrate equipped with a vacuum pump to remove the significant build-up of the sheath solution overflow, drastically limiting the ultimate 3D printing resolution. Harnessing the aforementioned microfluidic printhead and a fibrin-based biomaterial, the fabrication of a functional neural tissue model using induced pluripotent stem cells (iPSCs)[186] or mesenchymal stem cells (MSCs)[190] along with a 3D-printed glioblastoma multiforme (GBM) model[191,192] was reported (Figure 7e). To increase the model complexity, the same bioink was loaded with guggulsterone-releasing microspheres to encourage stem cell differentiation,[193] boosting the mechanical strength of the final 3D construct as well as the bioink printability.[194] Using the same commercial microfluidic printhead, another study reported the successful printing of smooth muscle cells with high viability.[195]

The serial combination of flow-focusing junctions makes microfluidic printheads suitable for core-shell fibers biofabrication, overcoming the technical limitations of multiple coaxial needles. A 3D *in vitro* kidney model was created by Addario *et al.* to investigate renal physiopathological conditions[196] (Figure 7f). Core-shell fibers are produced through two serial T-junctions, one to surround renal tubule-derived primary cells with HUVECs and one to crosslink the filament with a $CaCl_2$-based solution. After 14 days, a tubular structure following the natural cell rearrangement observed in the renal tissue is formed.

The microfluidic approach creates countless solutions to increase the complexity of printed constructs by controlling both biomaterial and cell deposition. Serex *et al.* recently suggested a set of smart microfluidic printheads to perform (i) multi-material printing, (ii) flow focusing, (iii) mixing of biomaterial inks, and (iv) cell concentration.[197] In the first case, fast switching (500 ms) and seamless transition both between alginate-based materials and photocrosslinkable resins were achieved. By alternating inks with different Young's moduli, the authors demonstrated the possibility to create thin slabs with patterned mechanical properties. The flow-focusing geometry, instead, was employed to extrude alginate fibers crosslinked using a calcium chloride solution as sheath fluid, resulting in fiber diameters between 200 and 800 μm. However, only single-layer structures could be printed, suggesting that the deposition of additional layers was hindered by the excessive crosslinking solution gathered around the fibers. Finally, a unique approach to adjust printed cell concentration on-the-fly was proposed using a microfluidic cell concentrator.[198] The latter consisted of a main channel fitted with micropillars on the sides at a fixed distance of 1.5 μm. Excess liquid was drained from the main channel after imposing a negative flow from a secondary inlet, thereby creating a colander-like filtering system.

In this way, NOR-10 fibroblasts initially injected at a density of 2×10^6 cells/ml reached a final concentration of 20×10^6 cells/ml and were subsequently embedded in collagen using a passive micromixer. Despite the adopted solution enabling high cell density printing while guaranteeing 97% of cell viability, further improvements are required to enhance the resolution of the ultimate construct and the deposition of multiple layers.

Even though a3DMB is ushering in a new paradigm for extrusion-based biofabrication, this technology has not gained traction among biofabrication communities since most monolithic microfluidic printheads still do not achieve the deposition accuracy of conventional extrusion bioprinters. Moreover, owing to the extreme sensitivity of such systems, manufacturing flaws or air bubbles present in microchannels induce flow disturbances that may alter the internal fluid patterns, compromising the stability of the spinning process and the accuracy of the entire printing. Moreover, since coaxial flow is not imposed by physical constraints but rather by hydrodynamic forces, the resulting cross-section of extruded fibers cannot depart from cylindrical-based geometries.[85]

5. Conclusions and future perspectives

The technological advancements achieved in manufacturing microfluidic chips have fostered the use of MST as a versatile approach for fabricating biological tissue models. Additionally, the incorporation of microfluidic printheads into 3D bioprinters has enabled the manufacture of 3D structures with a great degree of control, resolution, and

complexity. In light of this, microfluidic-enhanced 3D bioprinting ought to become an outstanding strategy to produce highly biomimetic human tissue substitutes in a single step, resembling physiological architecture from the nanometric (microarchitecture) up to the millimetric (macroarchitecture) scale. As addressed in this review, microfluidic technology does indeed provide high control over the inter- and intrafiber composition. The integration of microfluidic operators (e.g., combiners, splitter, mixers, and filters) not only enables the fabrication of multi-compartment and microhollowed fibers but also provides the possibility to modulate fiber composition and shape on-demand while printing, opening unlimited possibilities to realize hierarchical *in vitro* models of human tissues.

Recently, however, 3D biomanufacturing systems based on the extrusion of bioinks from metallic needles have been employed in the field of biofabrication, limiting the complexity and functionality of biological models obtained. In fact, the use of metallic connectors not only raises the amount of shear stress generated, which is detrimental for encapsulated cells,[140,188] but also restricts internal fluid handling. In fact, metallic parts are not transparent and represent physical constraints for fluid flowing, also increasing the possibility of disturbances of flow profiles. Moreover, manufacturing variability is often introduced since metallic elements are manually inserted within or at the outlet of microfluidic chips. In conclusion, even though the integration of a microfluidic chip enables the realization of more sophisticated 3D-printed biomodels, these issues must be taken into consideration when employing such platforms.

With advanced 3D microfluidic printheads, which are designed through CAD software and rapidly manufactured, manual fabrication steps are minimized, thus enhancing the quality of the final microdevice and the printing performances. In this context, connector-free microfluidic printheads can be designed to avoid the need for metallic needles, allowing for the extrusion of cell-laden fibers in a milder and damage-free manner. Indeed, compared to any other nozzle-based system, these biofabrication platforms not only enhance versatility of manufacturing but also increase viability of bioprinted constructs, a crucial aspect when printing high-sensitive cellular species or high-cell density bioinks.

a3DMB platforms are usually provided with a flow-focusing junction downstream and can be coupled with additional microfluidic units upstream to execute several operations on bioinks including mixing, splitting and cell concentration. In general, such microfluidic printheads are monolithic pieces of a transparent material (PDMS, PC, etc.); however, at the same time, these devices might also be built from standardized independent pieces, exploiting the idea of discrete microfluidics.[199,200] In this manner, multiple microfluidic components can be combined to form a single device using plastic tubes or other joining techniques, akin to the Lego® brick concept[201] or magnetic connectors.[202]

From a broader perspective, a considerable effort must be spent on scaling up the biofabrication process to produce compact macrotissues (or even organs) while maintaining the microarchitectural control offered by 3DMB. Printing larger structures with high cellular density requires tissue vascularization to ensure nutrients diffusion throughout the whole construct. Thus, we need to further expand the potential and versatility of microfluidic printheads to produce large dense tissues embedding vasculature—a complex network of multi-scale hollow structures. Last but not least, the clinical application of this technology requires a transition of 3DMB into a user-friendly system that can be operated also by non-specialized professional figures (i.e., doctors) so that it will become an instrument routinely employed in hospitals.

However, to date, 3DMB-based approaches are still poorly investigated and need improvements so that it will become a standard in biofabrication contexts. We envision that the potential for creating multi-layered, multi-core, hollow, and hierarchical fibers with real-time control on a single platform is limitless. In turn, the employment of microfluidic-assisted biofabrication systems will enable the engineering of more 3D functional structures that recapitulate the native environment to an unparalleled degree.

Acknowledgments

None.

Funding

G.C. acknowledges funding from AIRC Aldi Fellowship under grant agreement No. 25412. The research leading to these results was also supported by European Research Council Synergy grant ASTRA (n. 855923).

Conflict of interest

The authors declare no conflict of interest.

Author contributions

Conceptualization: Federico Serpe, Chiara Scognamiglio, Gianluca Cidonio

Methodology: Carlo Massimo Casciola, Giancarlo Ruocco

Writing – original draft: Federico Serpe, Chiara Scognamiglio

Writing – review & editing: Federico Serpe, Chiara Scognamiglio, Gianluca Cidonio, Carlo Massimo Casciola, Giancarlo Ruocco

Ethics approval and consent to participate

Not applicable.

Consent for publication

Not applicable.

Availability of data

Not applicable.

References

1. Whitesides GM. The origins and the future of microfluidics. *Nature.* 2006;442(7101):368-373. doi: 10.1038/nature05058
2. Convery N, Gadegaard N. 30 Years of microfluidics. *Micro Nano Eng.* 2019;2(November 2018):76-91. doi: 10.1016/j.mne.2019.01.003
3. Guimarães CF, Gasperini L, Marques AP, Reis RL. 3D flow-focusing microfluidic biofabrication: One-chip-fits-all hydrogel fiber architectures. *Appl Mater Today.* 2021;23:101013. doi: 10.1016/j.apmt.2021.101013
4. Abrishamkar A, Nilghaz A, Saadatmand M, Naeimirad M, deMello AJ. Microfluidic-assisted fiber production: Potentials, limitations, and prospects. *Biomicrofluidics.* 2022;16(6):1-32. doi: 10.1063/5.0129108
5. Pati F, Gantelius J, Svahn HA. 3D bioprinting of tissue/organ models. *Angew Chemie Int Ed.* 2016;55(15):4650-4665. doi: 10.1002/anie.201505062
6. van der Heide D, Cidonio G, Stoddart MJ, D'Este M. 3D printing of inorganic-biopolymer composites for bone regeneration. *Biofabrication.* 2022;14(4):042003. doi: 10.1088/1758-5090/ac8cb2
7. Scognamiglio C, Soloperto A, Ruocco G, Cidonio G. Bioprinting stem cells: Building physiological tissues one cell at a time. *Am J Physiol - Cell Physiol.* 2020;319(3):C465-C480. doi: 10.1152/ajpcell.00124.2020
8. Cidonio G, Glinka M, Kim Y-H, Dawson JI, Oreffo ROC. Nanocomposite clay-based bioinks for skeletal tissue engineering. *Methods Mol Biol.* 2021;2147:63-72. doi: 10.1007/978-1-0716-0611-7_6
9. Memic A, Navaei A, Mirani B, et al. Bioprinting technologies for disease modeling. *Biotechnol Lett.* 2017;39(9):1279-1290. doi: 10.1007/s10529-017-2360-z
10. Iafrate L, Benedetti MC, Donsante S, et al. Modelling skeletal pain harnessing tissue engineering. *Vitr Model.* 2022;1(4-5):289-307. doi: 10.1007/s44164-022-00028-7
11. Marcotulli M, Tirelli MC, Volpi M, Jaroszewicz J. Microfluidic 3D printing of emulsion ink for engineering porous functionally graded materials. *Adv Mater Technol.* 2022;2201244:1-12. doi: 10.1002/admt.202201244
12. Davoodi E, Sarikhani E, Montazerian H, et al. Extrusion and microfluidic-based bioprinting to fabricate biomimetic tissues and organs. *Adv Mater Technol.* 2020;5(8): 1901044. doi: 10.1002/admt.201901044
13. Sackmann EK, Fulton AL, Beebe DJ. The present and future role of microfluidics in biomedical research. *Nature.* 2014;507(7491):181-189. doi: 10.1038/nature13118
14. Chen L, Yang C, Xiao Y, et al. Millifluidics, microfluidics, and nanofluidics: manipulating fluids at varying length scales. *Mater Today Nano.* 2021;16:100136. doi: 10.1016/j.mtnano.2021.100136
15. Bezrukov AN, Galyametdinov YG. Evaluation of diffusion coefficients of small ions in a microfluidic channel. 2021;85(8):889-893. doi: 10.3103/S1062873821080049
16. Böke JS, Kraus D, Henkel T. Microfluidic network simulations enable on-demand prediction of control parameters for operating lab-on-a-chip-devices. *Processes.* 2021;9(8):1320. doi: 10.3390/pr9081320
17. Qin D, Xia Y, Rogers JA, Jackman RJ, Zhao X-M, Whitesides GM. Microfabrication, microstructures and microsystems. In: Manz A, Becker H, eds. *Microsystem Technology in Chemistry and Life Sciences*. 1998;Vol 194 Springer-Verlag. 1-20. doi: 10.1007/3-540-69544-3_1
18. Xia Y, Whitesides GM. Soft lithography. *Angew Chemie - Int Ed.* 1998;37(5):550-575. doi: 10.1002/(sici)1521-3773(19980316)37:5<550::aid-anie550>3.3.co;2-7
19. O'Neill PF, Ben Azouz A, Vázquez M, et al. Advances in three-dimensional rapid prototyping of microfluidic devices for biological applications. *Biomicrofluidics.* 2014;8(5):052112. doi: 10.1063/1.4898632
20. Qin D, Xia Y, Whitesides GM. Soft lithography for micro- and nanoscale patterning. *Nat Protoc.* 2010;5(3): 491-502. doi: 10.1038/nprot.2009.234
21. Bhattacharjee N, Urrios A, Kang S, Folch A. The upcoming 3D-printing revolution in microfluidics. *Lab Chip.* 2016;16(10):1720-1742. doi: 10.1039/c6lc00163g

22. Thaweskulchai T, Schulte A. A low-cost 3-in-1 3d printer as a tool for the fabrication of flow-through channels of microfluidic systems. *Micromachines.* 2021;12(8):947. doi: 10.3390/mi12080947

23. Zhu F, Friedrich T, Nugegoda D, Kaslin J, Wlodkowic D. Assessment of the biocompatibility of three-dimensional-printed polymers using multispecies toxicity tests. *Biomicrofluidics.* 2015;9(6):61103. doi: 10.1063/1.4939031

24. MacDonald NP, Zhu F, Hall CJ, et al. Assessment of biocompatibility of 3D printed photopolymers using zebrafish embryo toxicity assays. *Lab Chip.* 2016;16(2): 291-297. doi: 10.1039/c5lc01374g

25. Joseph Rey JRH, Chen Q, Maalihan RD, et al. 3D printing of biomedically relevant polymer materials and biocompatibility. *MRS Commun.* 2021;11(2):197-212. doi: 10.1557/s43579-021-00038-8

26. de Almeida Monteiro Melo Ferraz M, Nagashima JB, Venzac B, Le Gac S, Songsasen N. 3D printed mold leachates in PDMS microfluidic devices. *Sci Rep.* 2020;10(1):994. doi: 10.1038/s41598-020-57816-y

27. Zhou Z, Chen D, Wang X, Jiang J. Milling positive master for polydimethylsiloxane microfluidic devices: The microfabrication and roughness issues. *Micromachines.* 2017;8(10). doi: 10.3390/mi8100287

28. Guckenberger DJ, De Groot TE, Wan AMD, Beebea DJ, Young EWK. Micromilling: A method for ultra-rapid prototyping of plastic microfluidic devices. *Lab Chip.* 2015;15(11): 2364-2378. doi: 10.1039/c5lc00234f

29. Ku X, Zhang Z, Liu X, Chen L. Low-cost rapid prototyping of glass microfluidic devices using a micromilling technique. *Microfluid Nanofluidics.* 2018;22(8):1-8. doi: 10.1007/s10404-018-2104-y

30. Hossain MM, Rahman T. Low cost micro milling machine for prototyping plastic microfluidic devices. *Proceedings.* 2018;2(13):707. doi: 10.3390/proceedings2130707

31. Virumbrales-Muñoz M, Livingston MK, Farooqui M, Skala MC, Beebe DJ, Ayuso JM. Development of a microfluidic array to study drug response in breast cancer. *Molecules.* 2019;24(23):1-12. doi: 10.3390/molecules24234385

32. Costantini M, Idaszek J, Szöke K, et al. 3D bioprinting of BM-MSCs-loaded ECM biomimetic hydrogels for in vitro neocartilage formation. *Biofabrication.* 2016;8(3):035002. doi: 10.1088/1758-5090/8/3/035002

33. Costantini M, Testa S, Mozetic P, et al. Microfluidic-enhanced 3D bioprinting of aligned myoblast-laden hydrogels leads to functionally organized myofibers in vitro and in vivo. *Biomaterials.* 2017;131:98-110. doi: 10.1016/j.biomaterials.2017.03.026

34. Idaszek J, Costantini M, Karlsen TA, et al. 3D bioprinting of hydrogel constructs with cell and material gradients for the regeneration of full-thickness chondral defect using a microfluidic printing head. *Biofabrication.* 2019;11(4):044101. doi: 10.1088/1758-5090/ab2622

35. Behroodi E, Latifi H, Bagheri Z, Ermis E, Roshani S, Moghaddam MS. A combined 3D printing/CNC micro-milling method to fabricate a large-scale microfluidic device with the small size 3D architectures: An application for tumor spheroid production. *Sci Rep.* 2020;10(1):1-14. doi: 10.1038/s41598-020-79015-5

36. Kyle S, Jessop ZM, Al-Sabah A, Whitaker IS. Printability of candidate biomaterials for extrusion based 3D printing: State-of-the-art. *Adv Healthc Mater.* 2017;6(16):1-16. doi: 10.1002/adhm.201700264

37. Waheed S, Cabot JM, Macdonald NP, et al. 3D printed microfluidic devices: Enablers and barriers. *Lab Chip.* 2016;16(11):1993-2013. doi: 10.1039/c6lc00284f

38. Macdonald NP, Cabot JM, Smejkal P, Guijt RM, Paull B, Breadmore MC. Comparing microfluidic performance of three-dimensional (3D) printing platforms. *Anal Chem.* 2017;89(7):3858-3866. doi: 10.1021/acs.analchem.7b00136

39. Ho CMB, Ng SH, Li KHH, Yoon Y-J. 3D printed microfluidics for biological applications. *Lab Chip.* 2015;15(18): 3627-3637. doi: 10.1039/c5lc00685f

40. Zeraatkar M, de Tullio MD, Pricci A, Pignatelli F. Exploiting limitations of fused deposition modeling to enhance mixing in 3D printed microfluidic devices. *Rapid Prototyp J.* 2021;27(10):1850-1859. doi: 10.1108/RPJ-03-2021-0051

41. Quero RF, Domingos Da Silveira G, Fracassi Da Silva JA, de Jesus DP. Understanding and improving FDM 3D printing to fabricate high-resolution and optically transparent microfluidic devices. *Lab Chip.* 2021;21(19):3715-3729. doi: 10.1039/d1lc00518a

42. Ballacchino G, Weaver E, Mathew E, et al. Manufacturing of 3d-printed microfluidic devices for the synthesis of drug-loaded liposomal formulations. *Int J Mol Sci.* 2021;22(15):8064. doi: 10.3390/ijms22158064

43. Mehta V, Vilikkathala Sudhakaran S, Rath SN. Facile route for 3D printing of transparent PETg-based hybrid biomicrofluidic devices promoting cell adhesion. *ACS Biomater Sci Eng.* 2021;7(8):3947-3963. doi: 10.1021/acsbiomaterials.1c00633

44. Mader M, Rein C, Konrat E, et al. 2021, Fused deposition modeling of microfluidic chips in transparent polystyrene. *Micromachines,* 12(11):1348.
doi: 10.3390/mi12111348

45. Kara A, Vassiliadou A, Ongoren B, et al. Engineering 3d printed microfluidic chips for the fabrication of nanomedicines. *Pharmaceutics.* 2021;13(12):1-17.
doi: 10.3390/pharmaceutics13122134

46. Ching T, Li Y, Karyappa R, Ohno A. Fabrication of integrated microfluidic devices by direct ink writing (DIW) 3D printing. *Sensors Actuators, B Chem.* 2019;297(December 2018):126609.
doi: 10.1016/j.snb.2019.05.086

47. Karyappa R, Ching T, Hashimoto M. Embedded ink writing (EIW) of polysiloxane inks. *ACS Appl Mater Interfaces.* 2020;12(20):23565-23575.
doi: 10.1021/acsami.0c03011

48. Childs EH, Latchman AV, Lamont AC, Hubbard J. Additive assembly for polyjet-based multi-material 3D printed microfluidics. *J Microelectromech Syst.* 2020;29(5): 1094-1096.
doi: 10.1109/JMEMS.2020.3003858

49. Walczak R, Adamski K. Inkjet 3D printing of microfluidic structures - On the selection of the printer towards printing your own microfluidic chips. *J. Micromech Microeng.* 2015;25(8):085013.
doi: 10.1088/0960-1317/25/8/085013

50. Hwang Y, Paydar OH, Candler RN. 3D printed molds for non-planar PDMS microfluidic channels. *Sensors Actuators, A Phys.* 2015;226:137-142.
doi: 10.1016/j.sna.2015.02.028

51. King PH, Jones G, Morgan H, de Planquea MRR, Zauner K-P. Interdroplet bilayer arrays in millifluidic droplet traps from 3D-printed moulds. *Lab Chip.* 2014;14(14):722-729.
doi: 10.1039/c3lc51072g

52. Glick CC, Srimongkol MT, Schwartz AJ, et al. Rapid assembly of multilayer microfluidic structures via 3D-printed transfer molding and bonding. *Microsyst Nanoeng.* 2016;2(1):16063.
doi: 10.1038/micronano.2016.63

53. Vijayan S, Parthiban P, Hashimoto M. Evaluation of lateral and vertical dimensions of micromolds fabricated by a polyjet™ printer. *Micromachines.* 2021;12(3):1-13.
doi: 10.3390/mi12030302

54. Anderson KB, Lockwood SY, Martin RS, et al. A 3D printed fluidic device that enables integrated features. *Anal Chem.* 2013;85(12):5622-5626.
doi: 10.1021/ac4009594

55. Chen S, He Z, Choi S, Novosselov IV. Characterization of inkjet-printed digital microfluidics devices. *Sensors.* 2021;21(9):3064.
doi: 10.3390/s21093064

56. Sochol RD, Sweet E, Glick CC, et al. 3D printed microfluidic circuitry via multijet-based additive manufacturing. *Lab Chip.* 2016;16(4):668-678.
doi: 10.1039/c5lc01389e

57. Layani M, Wang X, Magdassi S. Novel materials for 3D printing by photopolymerization. *Adv Mater.* 2018;30(41):1706344.
doi: 10.1002/adma.201706344

58. Lu Y, Mapili G, Suhali G, Chen S, Roy K. A digital micro-mirror device-based system for the microfabrication of complex, spatially patterned tissue. *J Biomed Mater Res.* 2006;77(2):396-405.
doi: 10.1002/jbm.a.30601

59. Männel MJ, Selzer L, Bernhardt R, et al. Optimizing process parameters in commercial micro- stereolithography for forming emulsions and polymer microparticles in nonplanar microfluidic devices. *Adv Mater Technol.* 2019;1800408: 1-10.
doi: 10.1002/admt.201800408

60. Qin D, Xia Y, Whitesides GM. Rapid prototyping of complex structures with feature sizes larger than 20 μm. *Adv Mater.* 1996;8(11):917-919.
doi: 10.1002/adma.19960081110

61. Bertsch A, Heimgartner S, Cousseau P, Renauda P. Static micromixers based on large-scale industrial mixer geometry. *Lab Chip.* 2001;1(1):56-60.
doi: 10.1039/b103848f

62. Morimoto Y, Kiyosawa M, Takeuchi S. Three-dimensional printed microfluidic modules for design changeable coaxial microfluidic devices. *Sens Actuators B Chem.* 2018;274(July):491-500.
doi: 10.1016/j.snb.2018.07.151

63. Costantini M, Testa S, Fornetti E, et al. Biofabricating murine and human myo-substitutes for rapid volumetric muscle loss restoration. *EMBO Mol Med.* 2021;13(3):1-17.
doi: 10.15252/emmm.202012778

64. Li W, Yao K, Tian L, Xue C, Zhang X, Gao X. 3D printing of heterogeneous microfibers with multi-hollow structure via microfluidic spinning. *J Tissue Eng Regen Med.* 2022;16(10):913-922.
doi: 10.1002/term.3339

65. Maruo S, Nakamura O, Kawata S. Three-dimensional microfabrication with two-photon-absorbed photopolymerization. *Opt Lett.* 1997;22(2):132-134.
doi: 10.1364/OL.22.000132

66. Faraji Rad Z, Prewett PD, Davies GJ. High-resolution two-photon polymerization: the most versatile technique for the fabrication of microneedle arrays. *Microsyst Nanoeng.* 2021;7(1):71.
doi: 10.1038/s41378-021-00298-3

67. Fornell A, Söderbäck P, Liu Z, De Albuquerque Moreira M, Tenje M. Fabrication of silicon microfluidic chips for acoustic

particle focusing using direct laser writing. *Micromachines.* 2020;11(2):113.
doi: 10.3390/mi11020113

68. Oliveira B, Veigas B, Fernandes AR, et al. Fast prototyping microfluidics: Integrating droplet digital lamp for absolute quantification of cancer biomarkers. *Sensors.* 2020;20(6):1624.
doi: 10.3390/s20061624

69. Yong J, Zhan Z, Singh SC, Chen F, Guo C. Microfluidic channels fabrication based on underwater superpolymphobic microgrooves produced by femtosecond laser direct writing. *ACS Appl Polym Mater.* 2019;1(11):2819-2825.
doi: 10.1021/acsapm.9b00269

70. Zyla G, Kovalev A, Esen C, Ostendorf A, Gorb S. Two-photon polymerization as a potential manufacturing tool for biomimetic engineering of complex structures found in nature. *J Opt Microsyst.* 2022;2(03):1-12.
doi: 10.1117/1.JOM.2.3.031203

71. Lölsberg J, Linkhorst J, Cinar A, Jans A, Kuehne AJC, Wessling M. 3D nanofabrication inside rapid prototyped microfluidic channels showcased by wet-spinning of single micrometre fibres. *Lab Chip.* 2018;18(9):1341-1348.
doi: 10.1039/c7lc01366c

72. Wang Y, Kankala RK, Zhu K, Wang S-B, Zhang YS, Chen A-Zg. Coaxial extrusion of tubular tissue constructs using a gelatin/GelMA blend bioink. *ACS Biomater Sci Eng.* 2019;5(10):5514-5524.
doi: 10.1021/acsbiomaterials.9b00926

73. Shao L, Gao Q, Zhao H, et al. Fiber-based mini tissue with morphology-controllable GelMA microfibers. *Small.* 2018;14(44):1-8.
doi: 10.1002/smll.201802187

74. Yu Y, Wei W, Wang Y, Xu C, Guo Y, Qin J. Simple spinning of heterogeneous hollow microfibers on chip. *Adv Mater.* 2016;28:6649-6655.
doi: 10.1002/adma.201601504

75. Hu M, Kurisawa M, Deng R, et al. Cell immobilization in gelatin – hydroxyphenylpropionic acid hydrogel fibers. *Biomaterials.* 2009;30(21):3523-3531.
doi: 10.1016/j.biomaterials.2009.03.004

76. Yang Y, Sun J, Liu X, et al. Wet-spinning fabrication of shear-patterned alginate hydrogel microfibers and the guidance of cell alignment. *Regen Biomater.* 2017;4(5):299-307.
doi: 10.1093/rb/rbx017

77. Zhang X, Weng L, Liu Q, Li D, Deng B. Facile fabrication and characterization on alginate microfibres with grooved structure via microfluidic spinning. *R Soc Open Sci.* 2019;6(5):181928.
doi: 10.1098/rsos.181928

78. Rinoldi C, Costantini M, Kijeńska-Gawrońska E, et al. Tendon tissue engineering:Effects of mechanical and biochemical stimulation on stem cell alignment on cell-laden hydrogel yarns. *Adv Healthc Mater.* 2019; 8(7):1-10.
doi: 10.1002/adhm.201801218

79. Xu Z, Wu M, Ye Q, Chen D, Liu K, Bai H. Spinning from nature: Engineered preparation and application of high-performance bio-based fibers. *Engineering.* 2022;14:100-112.
doi: 10.1016/j.eng.2021.06.030

80. Colosi C, Costantini M, Barbetta A, et al. Microfluidic bioprinting of heterogeneous 3d tissue constructs. *Methods Mol Biol.* 2017;1612:369-380.
doi: 10.1007/978-1-4939-7021-6_26

81. Wang G, Jia L, Han F, et al. Microfluidics-based fabrication of cell-laden hydrogel microfibers for potential applications in tissue engineering. *Molecules.* 2019;24(8).
doi: 10.3390/molecules24081633

82. Wu F, Ju X jie, He X heng, et al. A novel synthetic microfiber with controllable size for cell encapsulation and culture. *J Mater Chem B.* 2016;4:2455-2465.
doi: 10.1039/c6tb00209a

83. Onoe H, Okitsu T, Itou A, et al. Metre-long cell-laden microfibres exhibit tissue morphologies and functions. *Nat Mater.* 2013;12(6):584-590.
doi: 10.1038/nmat3606

84. Hu M, Deng R, Schumacher KM, et al. Hydrodynamic spinning of hydrogel fibers. *Biomaterials.* 2010;31(5):863–869.
doi: 10.1016/j.biomaterials.2009.10.002

85. Bonhomme O, Leng J, Colin A. Microfluidic wet-spinning of alginate microfibers: A theoretical analysis of fiber formation. *Soft Matter.* 2012;8(41):10641-10649.
doi: 10.1039/c2sm25552a

86. Kurdzinski ME, Gol Berrak, Hee AC, et al. Dynamics of high viscosity contrast confluent microfluidic flows. *Sci Rep.* 2017;7(1):1-11.
doi: 10.1038/s41598-017-06260-6

87. Zaeri A, Zgeib R, Cao K, Zhang F, Chang RC. Numerical analysis on the effects of microfluidic-based bioprinting parameters on the microfiber geometrical outcomes. *Sci Rep.* 2022;12(1):1-16.
doi: 10.1038/s41598-022-07392-0

88. Zhao M, Liu H, Zhang X, Wang H, Taoab T, Qin J. A flexible microfluidic strategy to generate grooved microfibers for guiding cell alignment. *Biomater Sci.* 2021;9(14):4880-4890.
doi: 10.1039/D1BM00549A

89. Cai J, Ye D, Wu Y, Fan L, Yu H. Injectable alginate fibrous hydrogel with a three-dimensional network structure fabricated by microfluidic spinning. *Compos Commun.* 2019;15(April):1-5.
doi: 10.1016/j.coco.2019.06.004

90. Ebrahimi M, Ostrovidov S, Bae H, Kim SB, Bae H, Khademhosseini A. Enhanced skeletal muscle formation on microfluidic spun gelatin methacryloyl (GelMA) fibres using surface patterning and agrin treatment. *J Tissue Eng Regenrative Med.* 2019;12:2151-2163.
doi: 10.1002/term.2738

91. Daniele MA, Radom K, Ligler FS. Microfluidic fabrication of multiaxial microvessels via hydrodynamic shaping. *RSC Adv.* 2014;4:23440-23446. doi: 10.1039/c4ra03667k

92. Williams CG, Malik AN, Kim TK, Manson PN, Elisseeff JH. Variable cytocompatibility of six cell lines with photoinitiators used for polymerizing hydrogels and cell encapsulation. *Biomaterials.* 2005;26(11):1211-1218. doi: 10.1016/j.biomaterials.2004.04.024

93. Lim KS, Klotz BJ, Lindberg GCJ, et al. Visible light cross-linking of gelatin hydrogels offers an enhanced cell microenvironment with improved light penetration depth. *Macromol Biosci.* 2019;19(6):1-14. doi: 10.1002/mabi.201900098

94. He X, Wang W, Deng K, et al. Microfluidic fabrication of chitosan microfibers with controllable internals from tubular to peapodlike structures. *RSC Adv.* 2015;5: 928-936. doi: 10.1039/c4ra10696b

95. Cui T, Yu J, Li Q, et al. Large-scale fabrication of robust artificial skins from a biodegradable sealant-loaded nanofiber scaffold to skin tissue via microfluidic blow-spinning. *Adv Mater.* 2020;2000982(32):1-11. doi: 10.1002/adma.202000982

96. Jia J, Richards DJ, Pollard S, et al. Engineering alginate as bioink for bioprinting. *Acta Biomater.* 2014;10(10): 4323-4331. doi: 10.1016/j.actbio.2014.06.034

97. Hernández-González AC, Téllez-Jurado L, Rodríguez-Lorenzo LM. Alginate hydrogels for bone tissue engineering, from injectables to bioprinting: A review. *Carbohydr Polym.* 2020;229(October 2019):115514. doi: 10.1016/j.carbpol.2019.115514

98. Costantini M, Colosi C, Święszkowski W, Barbetta A. Co-axial wet-spinning in 3D bioprinting: State of the art and future perspective of microfluidic integration. *Biofabrication.* 2019;11(1):012001. doi: 10.1088/1758-5090/aae605

99. Du XY, Li Q, Wu G, Chen S. Multifunctionalmicro/nanoscale fibers based on microfluidic spinning technology. *Adv Mater.* 2019;31(52):1-38. doi: 10.1002/adma.201903733

100. Cidonio G, Costantini M, Pierini F, Scognamiglio C, Agarwald T, Barbetta A. 3D printing of biphasic inks: beyond single-scale architectural control. *J Mater Chem C.* 2021;9(37):12489-12508. doi: 10.1039/D1TC02117F

101. Sivashanmugam A, Arun Kumar R, Vishnu Priya M, Nair SV, Jayakumar R. An overview of injectable polymeric hydrogels for tissue engineering. *Eur Polym J.* 2015;72: 543-565. doi: 10.1016/j.eurpolymj.2015.05.014

102. Chopin-Doroteo M, Mandujano-Tinoco EA, Krötzsch E. Tailoring of the rheological properties of bioinks to improve bioprinting and bioassembly for tissue replacement. *Biochim Biophys Acta - Gen Subj.* 2021;1865(2):129782. doi: 10.1016/j.bbagen.2020.129782

103. Cooke ME, Rosenzweig DH. The rheology of direct and suspended extrusion bioprinting. *APL Bioeng.* 2021;5(1):011502. doi: 10.1063/5.0031475

104. Townsend JM, Beck EC, Gehrke SH, Berkland CJ, Detamore MS. Flow behavior prior to crosslinking: The need for precursor rheology for placement of hydrogels in medical applications and for 3D bioprinting. *Prog Polym Sci.* 2019;91:126-140. doi: 10.1016/j.progpolymsci.2019.01.003

105. Rudolph N, Osswald TA. *Polymer Rheology: Fundamentals and Applications*, Carl Hanser Verlag GmbH & Company KG; 2014. https://books.google.pl/books?id=11ctBQAAQBAJ

106. Bird RB, Armstrong RC, Hassager O. *Dynamics of Polymeric Liquids, Volume 1: Fluid Mechanics*, Wiley; 1987.

107. Doi M, Edwards SF. *The Theory of Polymer Dynamics*, Clarendon Press; 1986. https://books.google.pl/books?id=sAFQzQEACAAJ

108. Maxwell JC. On the dynamical theory of gases. *Philos Trans R Soc London.* 1867;157:49-88. http://www.jstor.org/stable/108968

109. Bird RB, Armstrong RC, Hassager O. *Dynamics of Polymeric Liquids, Volume 2: Kinetic Theory*, Wiley; 1987.

110. Pourmasoumi P, Moghaddam A, Mahand SN, et al. A review on the recent progress, opportunities, and challenges of 4D printing and bioprinting in regenerative medicine. *J Biomater Sci Polym Ed.* 2023;34(1):108-146. doi: 10.1080/09205063.2022.2110480

111. Paxton N, Smolan W, Böck T, Melchels F, Groll J, Jungst T. Proposal to assess printability of bioinks for extrusion-based bioprinting and evaluation of rheological properties governing bioprintability. *Biofabrication.* 2017;9(4):044107. doi: 10.1088/1758-5090/aa8dd8

112. Gregory T, Benhal P, Scutte A, et al. Rheological characterization of cell-laden alginate-gelatin hydrogels for 3D biofabrication. *J Mech Behav Biomed Mater.* 2022;136(September):105474. doi: 10.1016/j.jmbbm.2022.105474

113. Cooke ME, Rosenzweig DH. The rheology of direct and suspended extrusion bioprinting. *APL Bioeng.* 2021;5(1):011502. doi: 10.1063/5.0031475

114. Filippi M, Buchner T, Yasa O, Weirich S, Katzschmann RK. Microfluidic tissue engineering and bio-actuation. *Adv Mater.* 2022;34(23):2108427. doi: 10.1002/adma.202108427

115. Cheng Y, Yu Y, Fu F, et al. Controlled fabrication of bioactive microfibers for creating tissue constructs using microfluidic techniques. *ACS Appl Mater Interfaces.* 2016;8(2): 1080-1086.
doi: 10.1021/acsami.5b11445

116. Boyd DA, Shields AR, Howell PB, Ligler FS. Design and fabrication of uniquely shaped thiol–ene microfibers using a two-stage hydrodynamic focusing design. *Lab Chip.* 2013;13:3105-3110.
doi: 10.1039/c3lc50413a

117. Kobayashi A, Yamakoshi K, Yajima Y, Utoh R, Yamada M, Seki M. Preparation of stripe-patterned heterogeneous hydrogel sheets using micro fluidic devices for high-density coculture of hepatocytes and fibroblasts. *J Biosci Bioeng.* 2013;116(6):761-767.
doi: 10.1016/j.jbiosc.2013.05.034

118. Gursoy A, Iranshahi K, Wei K, et al. Facile fabrication of microfluidic chips for 3D hydrodynamic focusing and wet spinning of polymeric fibers. *Polymers (Basel).* 2020;12(3): 1-13.
doi: 10.3390/polym12030633

119. Attalla R, Ling C, Selvaganapathy P. Fabrication and characterization of gels with integrated channels using 3D printing with microfluidic nozzle for tissue engineering applications. *Biomed Microdevices.* 2016;18(1):17.
doi: 10.1007/s10544-016-0042-6

120. Wei D, Sun J, Bolderson J, et al. Continuous fabrication and assembly of spatial cell-laden fibers for a tissue-like construct via a photolithographic-based microfluidic chip. *ACS Appl Mater Interfaces.* 2017;9:14606-14617.
doi: 10.1021/acsami.7b00078

121. Pi Q, Maharjan S, Yan X, et al. Digitally tunable microfluidic bioprinting of multilayered cannular tissues. *Adv Mater.* 2018;30(43):1-10.
doi: 10.1002/adma.201706913

122. Xiao Y, Yang C, Zhai X, et al. Bioinspired tough and strong fibers with hierarchical core–shell structure. *Adv Mater Interfaces.* 2023;10(2):2201962.
doi: 10.1002/admi.202201962

123. Colosi C, Shin SR, Manoharan V, et al. Microfluidic bioprinting of heterogeneous 3D tissue constructs using low-viscosity bioink. *Adv Mater,* 2016;28(4):677-684.
doi: 10.1002/adma.201503310

124. Feng F, He J, Li J, Mao M, Li D. Multicomponent bioprinting of heterogeneous hydrogel constructs based on microfluidic printheads. *Int JBioprint.* 2019;5(2):39-48.
doi: 10.18063/ijb.v5i2.202

125. Miri AK, Nieto D, Iglesias L, et al. Microfluidics-enabled multimaterial maskless stereolithographic bioprinting. *Adv Mater.* 2018;30(27):1-9.
doi: 10.1002/adma.201800242

126. Hassan I, Selvaganapathy PR. Microfluidic printheads for highly switchable multimaterial 3D printing of soft materials. *Adv Mater Technol.* 2022;2101709:1-10.
doi: 10.1002/admt.202101709

127. Hardin JO, Ober TJ, Valentine AD, Lewis JA. Microfluidic printheads for multimaterial 3D printing of viscoelastic inks. *Adv Mater,* 2015;27(21):3279-3284.
doi: 10.1002/adma.201500222

128. Zhang L, Fu L, Zhang X, Chen L, Cai Q, Yang X. Hierarchical and heterogeneous hydrogel system as a promising strategy for diversified interfacial tissue regeneration. *Biomater Sci.* 2021;9(5):1547-1573.
doi: 10.1039/D0BM01595D

129. Chai N, Zhang J, Zhang Q, et al. Construction of 3D printed constructs based on microfluidic microgel for bone regeneration. *Compos Part B Eng.* 2021;223(June):109100.
doi: 10.1016/j.compositesb.2021.109100

130. Kamperman T, Henke S, van den Berg A, et al. Single cell microgel based modular bioinks for uncoupled cellular micro- and macroenvironments. *Adv Healthc Mater.* 2017;6(3):1600913.
doi: 10.1002/adhm.201600913

131. Kim B, Kim I, Choi W, Kim SW, Kim J, Lim G. Fabrication of cell-encapsulated alginate microfiber scaffold using microfluidic channel. *J Manuf Sci Eng.* 2008;130(2):0210161-0210166.
doi: 10.1115/1.2898576

132. Yao K, Li W, Li K, et al. Simple fabrication of multicomponent heterogeneous fibers for cell co-culture via microfluidic spinning. *Macromol Biosci.* 2020;20(3):1900395.
doi: 10.1002/mabi.201900395

133. Oh J, Kim K, Won SW, et al. Microfluidic fabrication of cell adhesive chitosan microtubes. *Biomed Microdevices.* 2013;15(3):465-472.
doi: 10.1007/s10544-013-9746-z

134. Novosel EC, Kleinhans C, Kluger PJ. Vascularization is the key challenge in tissue engineering. *Adv Drug Deliv Rev.* 2011;63(4-5):300-311.
doi: 10.1016/j.addr.2011.03.004

135. Cheng Y, Zheng F, Lu J, et al. Bioinspired multicompartmental microfibers from microfluidics. *Adv Mater,* 2014;26(30):5184-5190.
doi: 10.1002/adma.201400798

136. Cheng J, Jun Y, Qin J, Lee S-H. Electrospinning versus microfluidic spinning of functional fibers for biomedical applications. *Biomaterials.* 2017;114:121-143.
doi: 10.1016/j.biomaterials.2016.10.040

137. Jun Y, Kang E, Chae S, Lee S-H. Microfluidic spinning of micro- and nano-scale fibers for tissue engineering. *Lab Chip.* 2014;14(13):2145-2160.
doi: 10.1039/c3lc51414e

138. Kang E, Choi YY, Chae SK, Moon J-H, Chang J-Y, Lee S-H. Microfluidic spinning of flat alginate fibers with grooves for cell-aligning scaffolds. *Adv Mater.* 2012;24(31):4271-4277. doi: 10.1002/adma.201201232

139. Celikkin N, Presutti D, Maiullari F, et al. Combining rotary wet-spinning biofabrication and electro-mechanical stimulation for the in vitro production of functional myo-substitutes. *Biofabrication.* 2023;15(4):045012. doi: 10.1088/1758-5090/ace934

140. Cidonio G, Glinka M, Dawson JI, Oreffo ROC. The cell in the ink: Improving biofabrication by printing stem cells for skeletal regenerative medicine. *Biomaterials.* 2019;209(March):10-24. doi: 10.1016/j.biomaterials.2019.04.009

141. Jia L, Han F, Yang H, et al. Microfluidic fabrication of biomimetic helical hydrogel microfibers for blood-vessel-on-a-chip applications. *Adv Healthc Mater.* 2019;8(13):1-10. doi: 10.1002/adhm.201900435

142. van Genderen AM, Valverde MG, Capendale PE, et al. Co-axial printing of convoluted proximal tubule for kidney disease modeling. *Biofabrication.* 2022;14(4):044102. doi: 10.1088/1758-5090/ac7895

143. Xu H, Casillas J, Krishnamoorthy S, Xu C. Effects of Irgacure 2959 and lithium physical properties, and microstructure in 3D bioprinting of vascular-like constructs. *Biomed Mater.* 2020;15(5):055021. doi: 10.1088/1748-605X/ab954e

144. Wang M, Li W, Mille LS, et al. Digital light processing based bioprinting with composable gradients. *Adv Mater.* 2022;34(1):2107038. doi: 10.1002/adma.202107038

145. Hogan J, Sun Y, Yu K, et al. Modeling the printability of photocuring and strength adjustable hydrogel bioink during projection-based 3D bioprinting. *J Manuf Process.* 2021;69:583-592. doi: 10.1088/1758-5090/aba413

146. Xie X, Wu S, Mou S, Guo N, Wang Z, Sun J. Microtissue-based bioink as a chondrocyte microshelter for DLP bioprinting. *Adv Healthc Mater.* 2022;11(22):2201877. doi: 10.1002/adhm.202201877

147. Guifang G, Tomo Y, Karen H, Dai G, Cui X. Inkjet-bioprinted acrylated peptides and PEG hydrogel with human mesenchymal stem cells promote robust bone and cartilage formation with minimal printhead clogging. *Biotechnol J.* 2015;10(10):1568-1577. doi: 10.1002/biot.201400635

148. Park JA, Yoon S, Kwon J, et al. Freeform micropatterning of living cells into cell culture medium using direct inkjet printing. *Sci Rep.* 2017;7(1):14610. doi: 10.1038/s41598-017-14726-w

149. Solis LH, Ayala Y, Portillo S, Varela-Ramirez A, Aguilera R, Boland T. Thermal inkjet bioprinting triggers the activation of the VEGF pathway in human microvascular endothelial cells in vitro. *Biofabrication.* 2019;11(4):045005. doi: 10.1088/1758-5090/ab25f9

150. Saadi MASR, Maguire A, Pottackal NT, et al. Direct ink writing: A 3D printing technology for diverse materials. *Adv Mater.* 2022;34(28):1-57. doi: 10.1002/adma.202108855

151. Jung Y, Shafranek RT, Tsui JH, Walcott J, Nelson A, Kim D-H. 3D bioprinting of mechanically tuned bioinks derived from cardiac decellularized extracellular matrix. *Acta Biomater.* 2021;119: 75-88. doi: 10.1016/j.actbio.2020.11.006

152. Connell CDO, Konate S, Onofrillo C, et al. Bioprinting free-form co-axial bioprinting of a gelatin methacryloyl bio-ink by direct in situ photo-crosslinking during extrusion. *Bioprinting.* 2020;19(April):e00087. doi: 10.1016/j.bprint.2020.e00087

153. Bertlein S, Brown G, Lim KS, et al. Thiol–ene clickable gelatin: A platform bioink for multiple 3D biofabrication technologies. *Adv Mater.* 2017;29(44):1-6. doi: 10.1002/adma.201703404

154. Ooi HW, Mota C, ten Cate AT, Calore A, Moroni L, Baker MB. Thiol–ene alginate hydrogels as versatile bioinks for bioprinting. *Biomacromolecules.* 2018;19(8):3390-3400. doi: 10.1021/acs.biomac.8b00696

155. Bhattacharyya A, Janarthanan G, Kim T, et al. Modulation of bioactive calcium phosphate micro/nanoparticle size and shape during in situ synthesis of photo-crosslinkable gelatin methacryloyl based nanocomposite hydrogels for 3D bioprinting and tissue engineering. *Biomater Res.* 2022;26(1):54. doi: 10.1186/s40824-022-00301-6

156. Rastin H, Ormsby RT, Atkins GJ, Losic D. 3D bioprinting of methylcellulose/gelatin-methacryloyl (MC/GelMA) bioink with high shape integrity. *ACS Appl Bio Mater.* 2020;3(3):1815-1826. doi: 10.1021/acsabm.0c00169

157. Bertassoni LE, Cardoso JC, Manoharan V, et al. Direct-write bioprinting of cell-laden methacrylated gelatin hydrogels. *Biofabrication.* 2014;6(2):024105. doi: 10.1088/1758-5082/6/2/024105

158. Romanazzo S, Molley TG, Nemec S, et al. Synthetic bone-like structures through omnidirectional ceramic bioprinting in cell suspensions. *Adv Funct Mater.* 2021;2008216:1-12. doi: 10.1002/adfm.202008216

159. Spencer AR, Sani ES, Soucy JR, et al. Bioprinting of a cell-laden conductive hydrogel composite. *ACS Appl Mater Interfaces.* 2019;11:30518-30533. doi: 10.1021/acsami.9b07353

160. Dikyol C, Altunbek M, Koc B. Embedded multimaterial bioprinting platform for biofabrication of biomimetic vascular structures. *J Mater Res.* 2021;36(19):3851-3864. doi: 10.1557/s43578-021-00254-x

161. Chalard A, Mauduit M, Souleille S, Joseph P, Malaquin L, Fitremann J. 3D printing of a biocompatible low molecular weight supramolecular hydrogel by dimethylsulfoxide water solvent exchange. *Addit Manuf.* 2020;33(February):101162. doi: 10.1016/j.addma.2020.101162

162. Colosi C, Costantini M, Latini R, et al. Rapid prototyping of chitosan-coated alginate scaffolds through the use of a 3D fiber deposition technique. *J Mater Chem B.* 2014;2(39): 6779-6791. doi: 10.1039/c4tb00732h

163. Duchi S, Onofrillo C, O'Connell CD, et al. Handheld co-axial bioprinting: Application to in situ surgical cartilage repair. *Sci Rep.* 2017;7(1):5837. doi: 10.1038/s41598-017-05699-x

164. Hakimi N, Cheng R, Leng L, et al. Handheld skin printer: In situ formation of planar biomaterials and tissues. *Lab Chip.* 2018;18(10):1440-1451. doi: 10.1039/c7lc01236e

165. Ying G, Manríquez J, Wu D, et al. An open-source handheld extruder loaded with pore-forming bioink for in situ wound dressing. *Mater Today Bio.* 2020;8(July):100074. doi: 10.1016/j.mtbio.2020.100074

166. Pagan E, Stefanek E, Seyfoori A, et al. A handheld bioprinter for multi-material printing of complex constructs. *Biofabrication.* 2023;15(3):035012. doi: 10.1088/1758-5090/acc42c

167. Salaris F, Colosi C, Brighi C, et al. 3D bioprinted human cortical neural constructs derived from induced pluripotent stem cells. *J Clin Med.* 2019;8(1595):1-13. doi: 10.3390%2Fjcm8101595

168. Yu Y, Shang L, Guo J, Wang J, Zhao Y. Design of capillary microfluidics for spinning cell-laden microfibers. *Nat Protoc.* 2018;13(11):2557-2579. doi: 10.1038/s41596-018-0051-4

169. Gao Q, He Y, Fu J, Liu A, Ma L. Coaxial nozzle-assisted 3D bioprinting with built-in microchannels for nutrients delivery. *Biomaterials.* 2015;61:203-215. doi: 10.1016/j.biomaterials.2015.05.031

170. Gao G, Park JY, Kim BS, Jang J, Cho D-W. Coaxial cell printing of freestanding, perfusable, and functional in vitro vascular models for recapitulation of native vascular endothelium pathophysiology. *Adv Healthc Mater.* 2018;7(23):1801102. doi: 10.1002/adhm.201801102

171. Wu Z, Cai H, Ao Z, Xu J, Heaps S, Guo F. Microfluidic printing of tunable hollow microfibers for vascular tissue engineering. *Adv Mater Technol.* 2021;6(8):1-9. doi: 10.1002/admt.202000683

172. Gao Q, Liu Z, Lin Z, et al. 3D bioprinting of vessel-like structures with multi-level fluidic channels 3D bioprinting of vessel-like structures with multi-level fluidic channels. *ACS Biomater Sci Eng.* 2017;3(3):399-408. doi: 10.1021/acsbiomaterials.6b00643

173. Wang D, Maharjan S, Kuang X, et al. Microfluidic bioprinting of tough hydrogel-based vascular conduits for functional blood vessels. *Sci Adv.* 2022;8(43):1-18. doi: 10.1126/sciadv.abq6900

174. Silva CA, Cortés-Rodriguez CJ, Hazur J, Reakasame S, Boccaccini AR. Rationaldesign of a triple-layered coaxial extruder system: In silico and in vitro evaluations directed towards optimizing cell viability. *Int JBioprint.* 2020;6(4): 96-105. doi: 10.18063/ijb.v6i4.282

175. Zuo Y, He X, Yang Y, et al. Microfluidic-based generation of functional microfibers for biomimetic complex tissue construction. *Acta Biomater.* 2016;38:153-162. doi: 10.1016/j.actbio.2016.04.036

176. Li S, Liu Y, Li Y, Sun Y, Hu Q. A novel method for fabricating engineered structures with branched micro-channel using hollow hydrogel fibers. *Biomicrofluidics.* 2016;10(6):064104. doi: 10.1063/1.4967456

177. Puertas-Bartolomé M, Włodarczyk-Biegun MK, del Campo A, Vázquez-Lasa B, Román JS. 3D printing of a reactive hydrogel bio-ink using a static mixing tool. *Polymers.* 2020;12(9):1986. doi: 10.3390/polym12091986

178. Fernando C, Johana E, Quevedo-moreno DA, et al. High-throughput and continuous chaotic bioprinting of spatially controlled bacterial microcosms. *ACS Biomater Sci Eng.* 2021;7:2192-2197. doi: 10.1021/acsbiomaterials.0c01646

179. Chávez-Madero C, de León-Derby MD, Samandari M, et al. Using chaotic advection for facile high-throughput fabrication of ordered multilayer micro- and nanostructures: Continuous chaotic printing. *Biofabrication.* 2020;12(3):35023. doi: 10.1088/1758-5090/ab84cc

180. Samandari M, Alipanah F, Majidzadeh-A K, Alvarez MM, Santiago GT-de, Tamayol A. Controlling cellular organization in bioprinting through designed 3D microcompartmentalization. *Appl Phys Rev.* 2021;8(2):1-14. doi: 10.1063/5.0040732

181. Guimarães CF, Gasperini L, Ribeiro RS, Carvalho AF, Marquesab AP, Reis RL. High-throughput fabrication of cell-laden 3D biomaterial gradients. *Mater Horizons.* 2020;7(9):2414-2421. doi: 10.1039/D0MH00818D

182. Lavrentieva A, Fleischhammer T, Enders A, Pirmahboub H, Bahnemann J, Pepelanova I. Fabrication of stiffness

gradients of GelMA hydrogels using a 3D printed micromixer. *Macromol Biosci.* 2020;20(7):e2000107. doi: 10.1002/mabi.202000107

183. Kuzucu M, Vera G, Beaumont M, et al. Extrusion-based 3D bioprinting of gradients of stiff ness, cell density, and immobilized peptide using thermogelling hydrogels. *ACS Biomater Sci Eng.* 2021;7:2192-2197. doi: 10.1021/acsbiomaterials.1c00183

184. Attalla R, Puersten E, Jain N, Selvaganapathy PR. 3D bioprinting of heterogeneous bi- and tri-layered hollow channels within gel scaffolds using scalable multi-axial microfluidic extrusion nozzle. *Biofabrication.* 2019;11(1):015012. doi: 10.1088/1758-5090/aaf7c7

185. Beyer ST, Bsoul A, Ahmadi A. 3D alginate constructs for tissue engineering printed using a coaxial flow focusing microfluidic device. In: *2013 Transducers & Eurosensors XXVII: The 17th International Conference on Solid-State Sensors, Actuators and Microsystems (TRANSDUCERS & EUROSENSORS XXVII),* IEEE. 2013;1206-1209. doi: 10.1109/TRANSDUCERS.2013.6626990

186. Abelseth E, Abelseth L, De La Vega L, Beyer ST, Wadsworth SJ, Willerth SM. 3D printing of neural tissues derived from human induced pluripotent stem cells using a fibrin-based bioink. *ACS Biomater Sci Eng.* 2019;5(1):234-243. doi: 10.1021/acsbiomaterials.8b01235

187. Mirani B, Stefanek E, Godau B, Hossein Dabiri SM, Akbari M. Microfluidic 3D printing of a photo-cross-linkable bioink using insights from computational modeling. *ACS Biomater Sci Eng.* 2021;7(7):3269-3280. doi: 10.1021/acsbiomaterials.1c00084

188. Akbari M, Khademhosseini A. Tissue bioprinting for biology and medicine. *Cell.* 2022;185(15):2644-2648. doi: 10.1016/j.cell.2022.06.015

189. Beyer ST, Mohamed T, Walus K. A microfluidics based 3D bioprinter with on-the-fly multimaterial switching capability. *17th Int Conf Miniaturized Syst Chem Life Sci MicroTAS.* 2013;1(October):176-178.

190. Perez MR, Sharma R, Masri NZ. 3D bioprinting mesenchymal stem cell-derived neural tissues using a fibrin-based bioink. *Biomolecules.* 2021;11(1250):1-15. doi: 10.3390/biom11081250

191. Lee C, Abelseth E, de la Vega L, Willerth SM. Bioprinting a novel glioblastoma tumor model using a fibrin-based bioink for drug screening. *Mater Today Chem.* 2019;12:78-84. doi: 10.1016/j.mtchem.2018.12.005

192. Smits IPM, Blaschuk OW, Willerth SM. Novel N-cadherin antagonist causes glioblastoma cell death in a 3D bioprinted co-culture model. *Biochem Biophys Res Commun.* 2020;529(2):162-168. doi: 10.1016/j.bbrc.2020.06.001

193. Sharma R, Smits IPM, De La Vega L, Lee C, Willerth SM. 3D bioprinting pluripotent stem cell derived neural tissues using a novel fibrin bioink containing drug releasing microspheres. *Front Bioeng Biotechnol.* 2020;8(February):1-12. doi: 10.3389/fbioe.2020.00057

194. Sharma R, Kirsch R, Valente KP, Perez MR, Willerth SM. Physical and mechanical characterization of fibrin-based bioprinted constructs containing drug-releasing microspheres for neural tissue engineering applications. *Processes.* 2021;9(7):1205. doi: 10.3390/pr9071205

195. Dickman CTD, Russo V, Thain K, et al. Functional characterization of 3D contractile smooth muscle tissues generated using a unique microfluidic 3D bioprinting technology. *FASEB J,* 2020;34(1):1652-1664. doi: 10.1096/fj.201901063RR

196. Addario G, Djudjaj S, Farè S, Boor P, Moroni L, Mota C. Microfluidic bioprinting towards a renal in vitro model. *Bioprinting.* 2020;20(July):e00108. doi: 10.1016/j.bprint.2020.e00108

197. Serex L, Bertsch A, Renaud P. Microfluidics: A new layer of control for extrusion-based 3D printing. *Micromachines.* 2018;9(2):86. doi: 10.3390/mi9020086

198. Serex L, Sharma K, Rizov V, Bertsch A, McKinney JD, Renaud P. Microfluidic-assisted bioprinting of tissues and organoids at high cell concentrations. *Biofabrication.* 2021;13(12). doi: 10.1088/1758-5090/abca80

199. Lee KG, Park KJ, Seok S, et al. 3D printed modules for integrated microfluidic devices. *RSC Adv.* 2014;4(62): 32876-32880. doi: 10.1039/c4ra05072j

200. Bhargava KC, Thompson B, Malmstadt N. Discrete elements for 3D microfluidics. *Proc Natl Acad Sci USA.* 2014;111(42):15013-15018. doi: 10.1073/pnas.1414764111

201. Vittayarukskul K, Lee AP. A truly Lego®-like modular microfluidics platform. *J MicromechMicroeng.* 2017; 27(3):35004. doi: 10.1088/1361-6439/aa53ed

202. Yuen PK. A reconfigurable stick-n-play modular microfluidic system using magnetic interconnects. *Lab Chip.* 2016;16(19):3700-3707. doi: 10.1039/c6lc00741d

203. Chae S, Kang E, Khademhosseini A, Lee SH. Micro/nanometer-scale fiber with highly ordered structures by mimicking the spinning process of silkworm. *Adv Mater.* 2013;25(22):3071-3078. doi: 10.1002/adma.201300837

204. Ahn SY, Mun CH, Lee SH. Microfluidic spinning of fibrous alginate carrier having highly enhanced drug loading capability and delayed release profile. *RSC Adv.* 2015;5:15172-15181.
doi: 10.1039/c4ra11438h

205. Sugimoto M, Kitagawa Y, Yamada M, Yajima Y, Utoha R, Sekia Minoru. Micropassage-embedding composite hydrogel fibers enable quantitative evaluation of cancer cell invasion under 3D coculture conditions. *Lab Chip.* 2018;18(9):1378-1387.
doi: 10.1039/C7LC01280B

206. Zhou X, Nowicki M, Sun H, et al. 3D bioprinting-tunable small-diameter blood vessels with biomimetic biphasic cell layers. *ACS Appl Mater Interfaces.* 2020;12(41): 45904-45915.
doi: 10.1021/acsami.0c14871